Bicontinuous microemulsion approach to design conducting composite materials for energy storage

Yelriza Yeszhan, Bachelor of Science

Submitted in fulfillment of the
requirements for the degree of Master
of Science
in Chemical and Materials Engineering

School of Engineering and Digital Sciences
Department of Chemical and Materials Engineering
Nazarbayev University

53 Kabanbay Batyr Avenue,
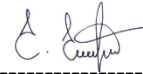Nur-Sultan, Kazakhstan, 010000

Supervisor: Dr. Nurxat Nuraje, Dr. Salimgerey Adilov

April, 2023

Abstract

In order to achieve good performance, it is important to control both the morphological and electrochemical characteristics of the electrode materials. In this regard, it is crucial to propose an appropriate synthesis technique. Among all conducting polymers, polyaniline attracts the most interest in the context of supercapacitors due to its ability to store energy via Faradaic processes.

This study reports a new facile approach for the synthesis of PANI nanofibers, as well as 3D architectural polymers and their composites. Characterization methods such as Infrared Fourier transform (FT-IR), scanning electron microscopy (SEM), thermogravimetric analysis (TGA), differential scanning calorimetry (DSC) Nitrogen adsorption has been used to study synthesized polyaniline-based materials. Furthermore, electrochemical approaches as electrochemical impedance spectroscopy (EIS), cyclic voltammetry (CV) and galvanostatic charge-discharge were applies to test performance of the polymer materials.

According to the results of the study, the PANI nanofiber exhibits pseudocapacitive behavior with a capacitance value of 280 F g^{-1} at a current density of 1 A g^{-1}. Futhermore, the material shows an energy density of 14 W h g^{-1} and a maximum power density of 900 μm W g^{-1}. Additionally, it should be noted that PANI retains about 98% of its original capacity after 1000 cycles. Thus, the PANI fiber electrode shows good cycling characteristics, suggesting the structural stability of the nanofibers. Even so, the PANI 3D supercapacitor has a low specific capacitance of 58.8 Fg^{-1} it was also stable and keep 98% of its capacitance after 637 cycles.

Acknowledgments

Table of contents

List of Abbreviations

1D	Three dimensional
2D	Two dimensional
3D	Three dimensional
AB	Acetylene black
AC	Alternating current
APS	Ammonium persulfate solution
BET	Brunauer-Emmett-Teller
CMC	Sodium carboxymethyl cellulose
CP	Conducting polymers
CPD	Charge potential difference
CV	Cyclic voltammetry
DC	Direct current
DSC	Differential Scanning Calorimetry
FT-IR	Fourier transform infrared
EC	Electrochemical capacitor
EDLC	Electric double-layer capacitors
EIS	Electrochemical impedance spectroscopy
ESR	Equivalent series resistance
GCD	Galvanostatic charge/discharge
HCL	Hydrochloric acid
NMP	N-methyl-2-pyrrolidone
OCP	Open circuit potential
PANI	Polyaniline
PEDOT	Poly(3,4-ethylenedioxythiophene)
PPY	Polypyrrole
PTh	Polythiophene
PVA	Poly(vinylalcohole)
PVDF	Poly(vinylidene fluoride)
SDS	Sodium dodecylsulfate

SEM	Scanning electron microscope
SS	Stainless steel
TGA	Thermogravimetric analysis

List of Figures

Chapter 1 – Introduction

The demands imposed by the existing environmental problems at present, associated with the depletion of fossil fuels and the greenhouse effect, are accelerating the development of new energy storage systems. These systems should allow, on the one hand, more efficient use of the energy of the current electricity distribution network, storing it during periods of low consumption to make it available during peak demand and, on the other, supplying the discontinuous nature of the new sources of renewable energy allowing a progressive increase in the amount of this energy that is integrated into the network. Moreover, the widespread use of consumer electronics products and the growing proliferation of new applications (such as electric vehicles, uninterruptible power supplies or solar energy transformation devices) whose operation requires the use of energy storage systems smaller, more powerful, and more efficient than the traditional ones but, at the same time, built from less polluting chemical components, it has also motivated research into new energy storage devices. Among the most studied systems currently for these purposes are capacitors, batteries, and fuel cells.
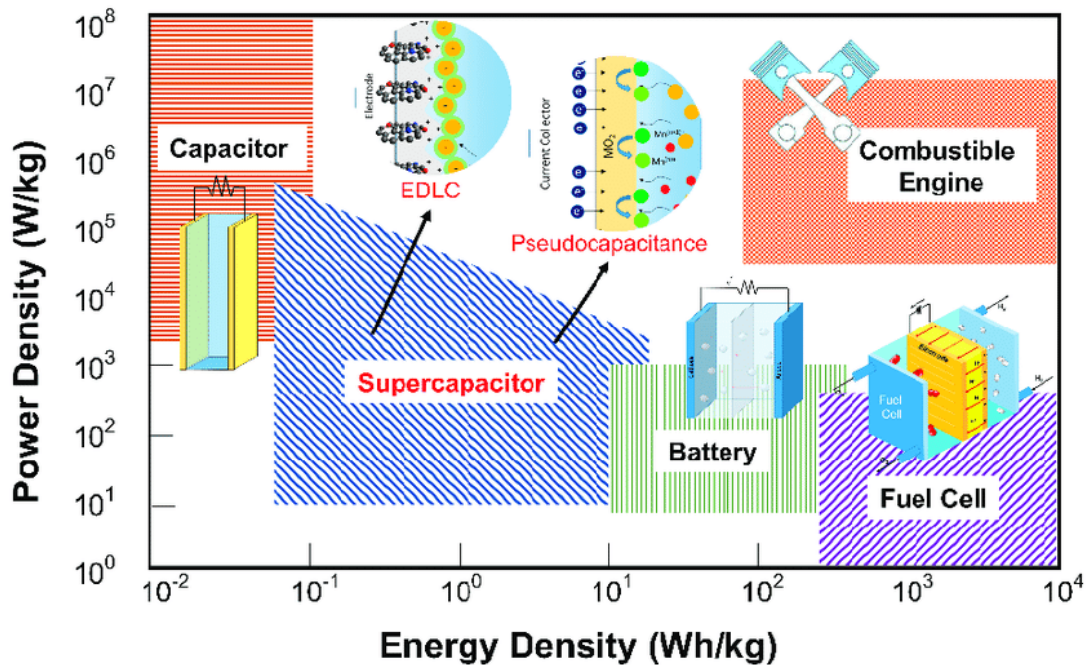
Figure 1-1. Ragone plot of energy storage devices [1]

The above-mentioned energy conversion and storage devices are shown in Figure 1-1, on the so-called "Ragon plot" [1], [2] in relation to their specific energies and capacities. As

can be seen from the figure, electrochemical capacitors or supercapacitors are located between traditional capacitors and batteries, since they simultaneously present high values of both energy density and power. Supercapacitors have a specific energy that is several orders of magnitude more than that of regular capacitors, allowing them to store 10 to 1000 times as much energy with less weight and volume [3], [4]. Although supercapacitors suffer from low energy densities, their power density is much higher than that of batteries and fuel cells. Therefore, it can be concluded that supercapacitors combine the power density characteristics of a battery with the energy density characteristics of a conventional capacitor [1].

Apart from the information presented by this type of diagram, it is necessary to consider other factors such as costs, cycle life, security, scalability etc. Although lithium-ion batteries are widely used in most current electronics due to their high charge densities (10-200Wh/kg), due to their low power densities (<1000 W/Kg), the fact that recharging them takes a long time (1-5 h), even unloading them is a slow process (0.3-3 h), as well as they present heating and dendrite formation after a few reuse cycles (1,000-10,000), giving rise to failures that finally result in security problems [4], [5], other systems capable of complementing and/or replacing them in certain applications are sought. For applications that require high power density (500-10,000 W/Kg), fast charge/discharge (s-min) and large reuse cycles (100,000-500,000), supercapacitors are recommended [2], [4]. Such is the case of backup power sources or regenerative brakes, which, instead of wasting energy in the form of heat, is converted into electrical energy [6]. The reason why supercapacitors do not dominate storage systems is their low charge density of 1–10 Wh/kg compared to batteries (∼200 Wh/kg) and fuel cells (∼350 Wh/kg [5]). Therefore, work continues increasing its energy density without compromising its power density or cyclic stability.

1.1 Aim of research

The main goal of this work is to design 1D and 3D conducting polymers and their composites through bicontinuous microemulsion approach and to understand the structure-property relation of these materials and explore their application in energy storage. The following objectives are pursued in this regard:

1. Synthesize 1D conductive polyaniline with high conductivity.

2. Design a freestanding 2D polymer film with good electrical conductivity and flexibility in order to compare with 1D polymer material.

3. Using crosslinker to produce 3D conducting polymer with enhanced surface area to increase capacitance.

4. Fabricate 3D polymer composite with high conductive material to improve conductivity.

5. Investigate the influence of the structure of these materials to its properties viachemical, mechanical and electrochemical methods.

6. Propose a design of energy storage device based on conducting polymer and its composite.

1.2 Hypothesis

Bicontinuous microemulsion system, where 1D, 3D polymers synthesized, can provide good environment to produce materials with both high surface area and conductivity.

1.3 The novelty of the research

This research will present a new and environmentally friendly approach to obtaining polymer composites based on bicontinuous microemulsions for further application in energy storage. The resulting material has outstanding electrochemical and mechanical properties since the presented method allows to control of the entire process by changing the concentration of one of the emulsion components and the reaction conditions. Considering that the proposed bicontinuous microemulsion approach is a fast and cheap method, it also can be used in industry.

1.4 Classification of supercapacitors

Electrochemical capacitors (EC) also known as supercapacitors (SC), offer properties (voltage, specific power, and operating costs) between batteries and conventional dielectric capacitors. These operate in a manner that is analogous to that of traditional capacitors in that they store electric charge; however, in contrast to traditional capacitors, the charge does not accrete on the two plates that are kept apart by the dielectric; rather, the charge stores at the interface between the conductor surface and an electrolyte [7]. Reversible mechanisms are used to store electrical energy and are classified depending on their capacitive behavior; a)

electrochemical double layer capacitors (EDLC), b) pseudocapacitance (PC) and c) asymmetrical capacitors (ASC), as shown in Figure 1-2.
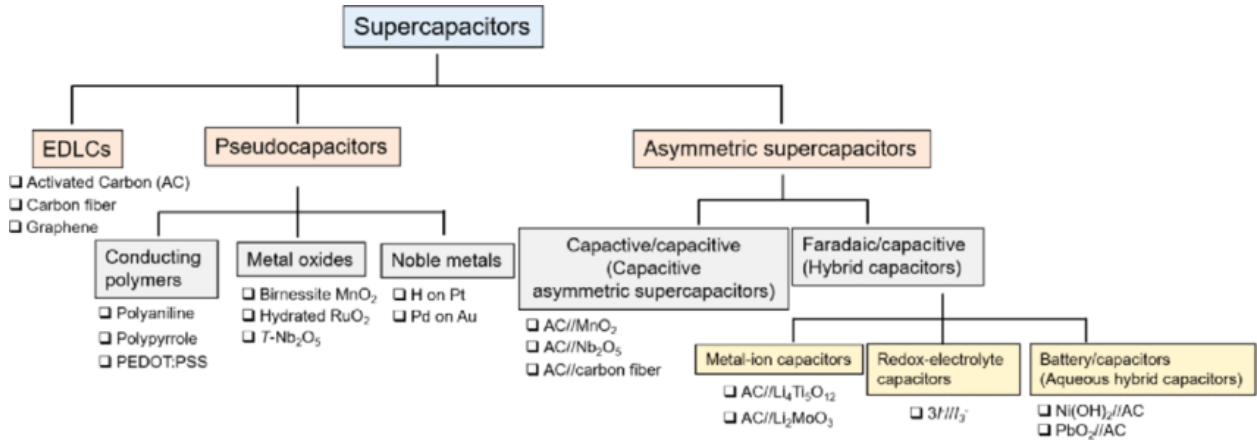
Figure 1-2. Classification of supercapacitors [8]

1.4.1 Electrical Double Layer Capacitor (EDLC)

EDLCs are charge storage devices constructed and assembled in a manner comparable to that of lithium-ion batteries. The design of EDLCs includes a separator, an electrolyte, and two electrodes. The separator provides an electrical barrier between the organic system's positive and negative electrodes in an organic electrolyte system [9].
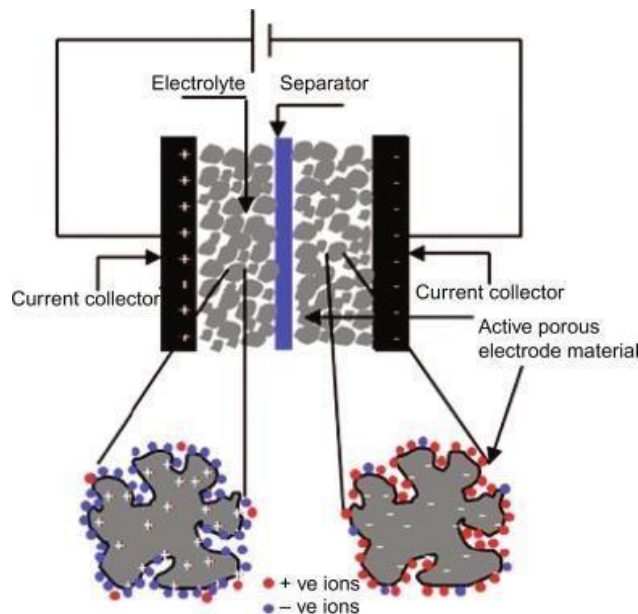
Figure 1-3. Schematic representation of EDLC [10]

The capacitance of the double layer is connected to the separation of electrical charges, which is obtained due to the alignment of ions and electrons at the interface of the electrode

and the electrolyte, as shown in Figure 1-3. Electrical charges build to an excess on the surface of either the cathode or the anode. Simultaneously, electrolyte ions that have compensating charges are accumulating in the electrolyte solution in order to keep the electrical potential in the system at a neutral state. During the process of charging the system, electrolyte cations migrate to the negative electrode, while electrolyte anions move to the positive electrode. Electrons move from the negative electrode to the positive electrode as they pass through the external circuit. The formation of a double layer at the interfaces with the electrodes is the end outcome of this process. After completion of the charging process, the positive ions on the electrode and the anions in the electrolyte are drawn to one another. This phenomenon is known as electrostatic attraction. The attraction that exists between the negative electrical charges that are present on the electrode and the cations that are present in the electrolyte is what helps to maintain the double layers that are present on the electrodes.The result is a voltage that is relatively stable. During the discharge procedure, the processes described above are inverted. Since the electrolyte content is the same whether the battery is being charged or discharged, this is the mechanism by which an electrical charge is created on the electrode surface. Consequently, energy accumulates at the interface between two strata [9], [11], [12].

1.4.2 Pseudocapacitors

Pseudocapacitors store energy through a reversible Faraday process, which is characterized by the possibility of electron transfer at the electrode-electrolyte and the presence of a double electrochemical layer, causing changes in the oxidation states of the electrode, but not a complete transformation of materials, as it occurs in a battery [13].

The pseudocapacitive behavior arises as a consequence of the existence of fast redox reactions that involve both the electrode and the electrolyte, in which, due to thermodynamic reasons, the charge necessary for the development of the electrode process is dependent on the potential, contrary to what happens in Nernstian ideal charge transfer processes [14]. As previously mentioned, capacitors that simultaneously combine the formation of the electrical double layer with the existence of faradaic reactions, or else store energy solely through pseudocapacitive processes, are called supercapacitors, ultracapacitors, or electrochemical capacitors. There are three types of electrochemical processes that can be used in the development of pseudocapacitive phenomena [15].

a) Those due to redox reactions of electroactive materials (e.g., RuO_2, IrO_2, etc.) or

electrochemically active surface groups present on the surface of carbon electrodes.

b) Those originated by electroadsorption processes, which occur as a consequence of the chemisorption of ions (generally anions, e.g., Cl⁻, I⁻, CNS⁻) or molecules, according to a process of the following type [16]:

$$M + A^- \leftrightarrow MA^{(1-\delta)} + \delta e^-$$

in which the quantity δe^- (or $1-\delta$) is related to the so-called "valence of electro adsorption" of the anion [16], which characterizes its behavior against chemisorption processes in electrodes.

c) The electrochemical doping of electrically conductive polymers.

The first two processes are strongly reliant on the features of the electrode surface since the mechanisms that cause them to occur are located on the surface of the electrode. The third procedure, on the other hand, uses the full volume of the polymeric material and, although being far less dependent on the surface properties of the electrode, still needs a certain percentage of mesopores in order to facilitate ion diffusion.

In general, both electrostatic and Faraday mechanisms of energy accumulation coexist in a supercapacitor; however, the supercapacitor's behavior is generally determined by only one of the two [17]In the case of carbon capacitors, the electrical double-layer mechanism predominates, whereas the opposite is true for capacitors with a transition metal or polymer electrodes.

1.4.3 Asymmetric supercapacitors

Asymmetric supercapacitors cover a broader range of SCs, taking as a distinction the types of electrodes used. Asymmetric supercapacitors refer to those SCs composed of different electrodes, so under this definition they can still be classified into two other groups: a) hybrids and b) two capacitive electrodes [18].
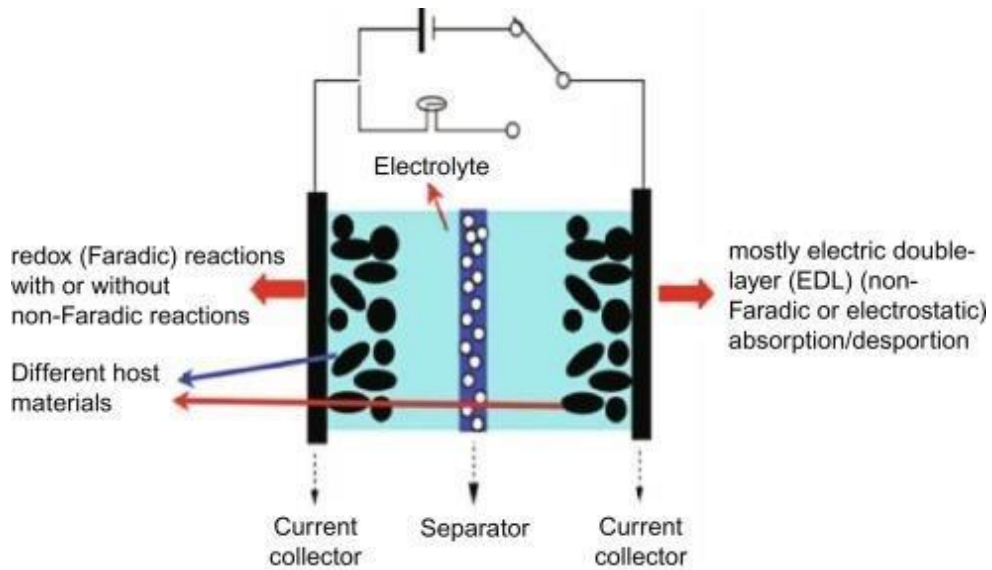
Figure 1-4. Construction of hybrid supercapacitor [19]

A hybrid capacitor is an invention that bridges the gap between a traditional capacitor and a battery. Due to the fact that hybrid capacitors' electrodes are made from a variety of materials, and charge accumulation is accomplished through a variety of processes, the term "hybrid" was coined to describe these devices. In the vast majority of hybrid capacitors, the cathode is composed of a material with pseudocapacitance (Figure 1-4). As a consequence of this, charge accumulates on the cathode as a result of redox processes, which leads to an increase in the specific capacitance of the capacitor and an expansion of the voltage range that it can operate at [20].

Hybrid energy storage systems are aimed at achieving performance comparable to batteries in terms of energy storage, as well as maintaining the high-power characteristics and good life of supercapacitors [19], [20].

1.5 Electrode materials for supercapacitors

The choice of electrode material in a supercapacitor is one of the most important factors in determining its electrochemical characteristics. This is because the process by which the device stores energy is typically governed by the type of electrode material used. These may be separated into three primary types according to the active material that they present: capacitors that are constructed with electrodes composed of carbon materials, capacitors that are constructed with transition metal oxides, and capacitors that employ conducting polymers. Each of these can be divided down further into subcategories.

1.5.1 Porous carbon materials

Carbon materials are the most widely used and most technologically implemented in the manufacture of electrodes for electrochemical capacitors such as consequence of an excellent combination of physical and chemical properties: (i) low cost, (ii) high surface area, (iii) availability, (iv) easy processing, (v) good thermal and chemical stability, (vi) high conductivity and (vii) great variety of shapes (powders, fibers, felts, composites, nanotubes, etc.) [21].

Charge storage in this type of capacitors is predominantly capacitive although, in general, there may be additional pseudocapacitive contributions due to polar functional groups present on the surface of the carbon material. Among the carbon materials most widely used as supercapacitor electrodes are activated carbons, mesoporous materials obtained from templates, carbon nanotubes, aerogels and xerogels, and carbon fibers [21].

1.5.2 Transition metal oxides

The capacitance that can be observed in electrode materials made from metal oxides is primarily attributable to the pseudocapacitive contribution. When compared to substances that have a higher surface area, such as carbon compounds, the double layer capacity of oxides is quite low since oxides have a very small surface area [22].

In order to be used as electrodes in supercapacitors, metal oxides need to possess good electronic conductivity, low crystalline ordering, and consist of metals that are in a variety of oxidation states. These metals must also be capable of inducing reversible redox reactions due to the electronic configuration and chemical nature of their molecules over a large voltage range [23].

1.5.3 Conducting polymers

Conducting polymers are materials with conjugated structures, in which the carbon chains of the polymer are formed by a sequence of single and double or triple conjugated bonds. In this type of materials, charge storage arises as a consequence of fast and reversible oxidation and reduction processes, related to the presence of conjugated π orbitals in their structure [24].Therefore, the energy storage in supercapacitors based on this type of materials has a Faradaic origin. Figure 1.13 illustrates the charge storage process of conductive polymers,

consisting of p-type or n-type electrochemical doping processes in which anions or cations - from electrolyte- are incorporated into the polymer. when it is oxidized or reduced, respectively [25].
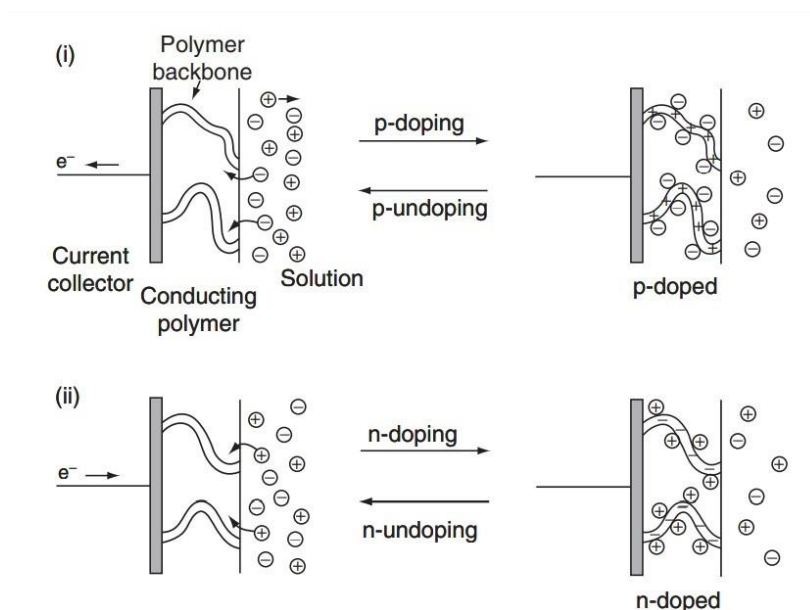
Figure 1-5. The operation principles of pseudocapacitor based on reversible doping processes: p-doping (i) and n-doping (ii) [25]

The aforementioned charging processes can be represented through the following two equations:

$$P \xrightarrow[X^+A^-]{\text{Oxidation}} P:X^+/A^- \qquad \text{p-type}$$

$$P \xrightarrow[X^+A^-]{\text{Reduction}} P:A^-/X^+ \qquad \text{n-type}$$
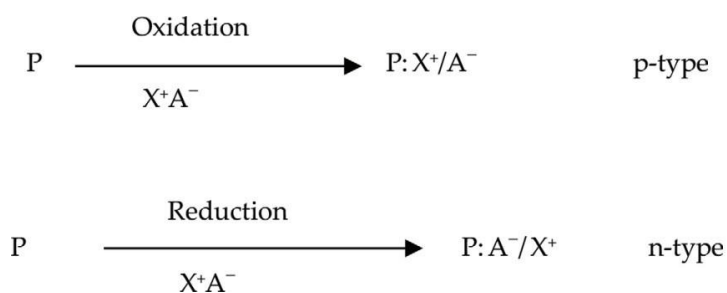
in which P represents the conducting polymer and A^- and X^+, an anion and a cation, respectively. The reactions corresponding to the discharge processes coincide with the inverse reactions of the previous ones.

Polypyrrole (PPY), polyaniline (PANI), and polythiophene (PTh) and their derivatives [24] (Fig. 1-6) are promising polymeric materials for use in supercapacitors among the most studied materials.
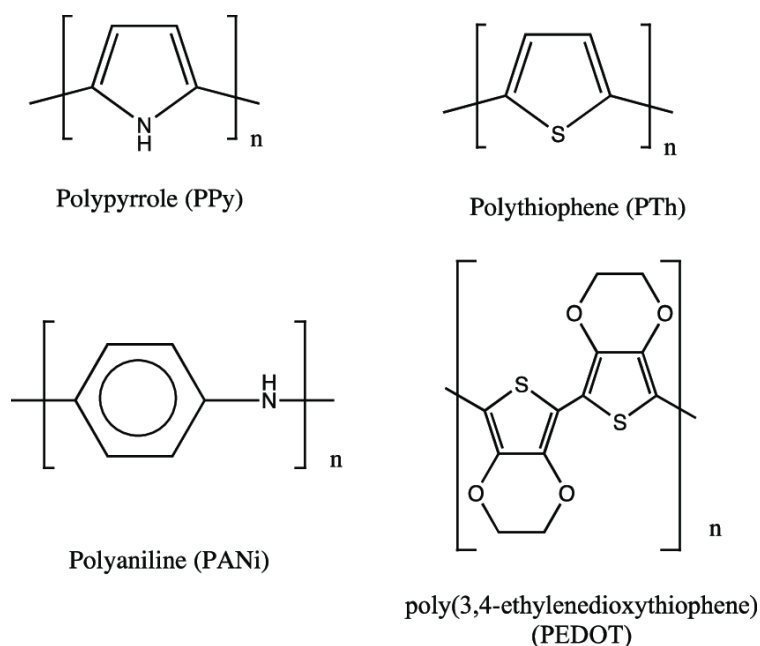
Figure 1-6. Structure of commonly used conducting polymers [24]

1.5.3.1 Polyaniline

The structure of this intrinsically conductive polymer is composed of the presence of benzenoid (presence of amine groups) and quinoid (presence of diimine groups) distributed throughout the polymeric chain. PANI possesses three oxidation states, being these called as the leucomeraldine form, which is the reduced form containing only benzenoid units in the polymer structure; the emerald form, which to the semi-oxidized/semi-reduced form with the presence of a quinoid ring per repetitive unit; and finally, the pernigraniline form, which contains two quinoid anises per repetitive unit, being considered the most oxidized form of PANI [26]. The different structures of the base forms of polyaniline are shown in Figure 1-7.
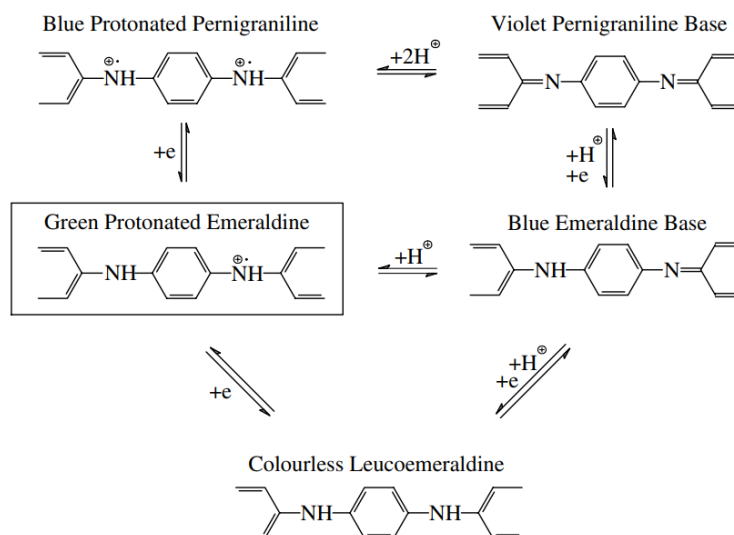
Figure 1-7. Different forms of polyaniline obtained from aniline polymerization [27]

The emeraldine form is what will result in the conductive form of PANI. However, emeraldine base (form represented in Figure 1-7) is insulating, and for it to make a change to the conductive form of the conjugated polymer, a process called doping must occur. This process occurs from the protonation of two nitrogen atoms diimine present in the polymeric chains when polyaniline is exposed to an acid. The protonated form of PANI is called emerald salt, and this process of protonation is accompanied by the change from blue to green color. The PANI doping process does not change the number of electrons in the polymer chain, differently from what happens for other conductive polymers [26]. In a first moment, a polymer is formed with the presence of bipolarons, characterized by the presence of localized dications of protonated diimine nitrogen. Through an internal redox reaction, a change of the bipolar structures occurs for the formation of two polarons (cation-radical), charge carriers that are directly related to the presence of more planar polymeric chains [27] and are responsible for the conductivity of electrons in na polymer structure. The transport of electrons in PANI occurs through a hopping mechanism between the crystalline regions. When the polar structures are formed, they act as holes (charge carriers) in the structure of the conjugated polymer. For electronic conductivity to occur, a non-nitrogenous located electron neighboring the polaron "jumps" to that entity, making it neutral and leaving a radical cation where before there was a neutral nitrogen. In this way, the electrons and holes move in successive "jumping" processes, raising an electrical conductivity along the polymer chain [26], [27].
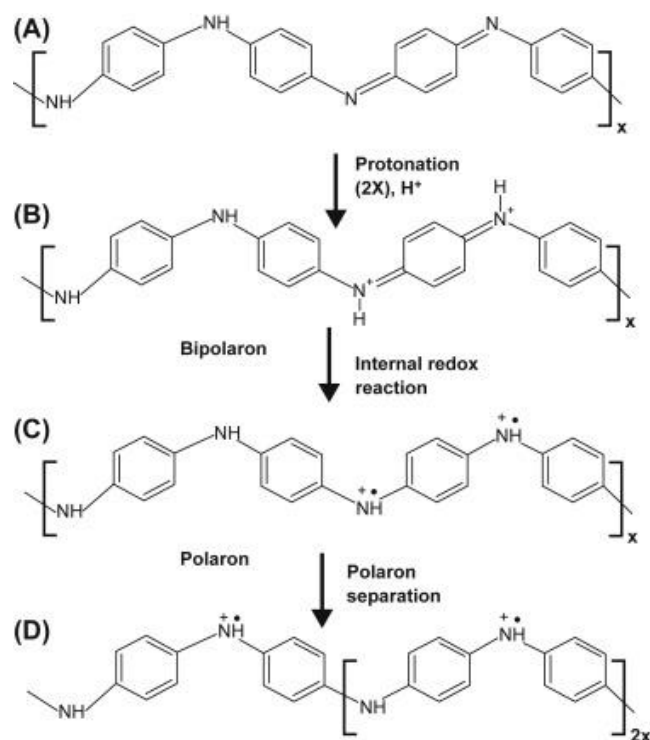
Figure 1-8. Protonation of polyaniline chains with formation of polarons and bipolarons [28]

As seen in Figure 1-8, the PANI protonation process is accompanied by the neutralization of the polymer charge by an oppositely charged counterion. This process results in the separation of charges and formation of the electrical double layer throughout the polymeric chain. The capacitive behavior of PANI results from this polymer protonation mechanism, and it is possible to state that the charged form is the one in which the chains are in the emeraldine salt form, and the uncharged form occurs in the reduction to the leucoemeraldine form [28].

1.5.3.2 PANI nanofibers

PANI nanofibers are characterized by having an elongated shape and a nanometric diameter (1D structure). These characteristics will vary according to the synthesis method used. The nanofibrillar morphology is said to be a type of intrinsic morphology of the oxidative synthesis of PANI [29]. At the interface of the nucleation points, the growth of the polymeric chains occurs, during a large part of the reaction time these nucleation points are suspended in the medium, and if the concentration of reactants is low and the acidity is high, the size of these particles tends to be nanometric. On these particles a certain number of polymeric chains will

begin to grow, which through the π-π interaction will tend to stack up to constitute the fiber. From this mechanism it is inferred that the smaller the particle, the thinner the nanofiber will be. The formation of nanofibers in interfacial polymerization could be explained by the formation of a layer of aniline cations that come from the organic phase and have become protonated when in contact with the acidic aqueous phase. The nanofibrillar PANI stands out for its high specific surface area that allows it to act as a chemical sensor [30] and an electrochemical condenser [29].

1.6 Fabrication of PANI based electrode

To manufacture electrode material for use in energy storage applications, PANI and its derivatives are an excellent choice due to the various benefits they offer in this regard. They are suitable for use as supercapacitor electrodes due to their low cost, environmental friendliness, high conductivity, wide voltage range, high storage capacity/porosity/reversibility, and controlled redox activity that can be achieved via chemical modification. The capacitive performance of PANI is maintained during the redox process. When the PANI is an oxidized state, the ions move to the backbone of the polymer; when it is reduced, the ions move away from the main backbone and back into the electrolyte solution. These reversible reactions occur not only on the surface of the polymer chains but also on the bulk of the chains. The charging and discharging processes are extremely reversible because the phenomena of charging and discharging are not related to structural alterations such as phase transitions [29].

1.6.1 Synthesis of PANI

Chemically, PANI can be produced in solutions that include monomers and oxidizing agents through a process known as synthesis. Oxidizing chemicals such as ferric chloride or ammonium persulfate can oxidize a monomer to generate a radical cation. This radical cation combines with another monomer or another cation to make a dimer. The formation of PANI requires multiple cycles of re-oxidation and coupling, which take place throughout the chain development process. Using this process, it is possible to produce the polymer in significant numbers [31]. In addition to chemical polymerization in the liquid phase, there is also polymerization in the vapor phase (also known as VPP). During the VPP process, monomer vapor makes its way to the substrate coated with oxidant, which then proceeds to polymerize and produce a polymer layer. The capacity of VPP to deposit thin PANI films on various substrates is the primary benefit of using this technique [32].

Electrochemical polymerization is an additional technology that can be used to produce polymers. This procedure is carried out in a solution containing a monomer, a doping agent, and possibly some more additives. When an anode potential is given to the conductive substrate, the monomer will begin to oxidize on the surface of the substrate. Anions are used to neutralize the positive charge that is carried by the chain of polymer molecules. For this oxidation process, the solvent, electrolyte salt, and substrate need to maintain their stable states [33].

1.7 Principle and method of experimental evaluation

Cyclic voltammetry (CV), galvanostatic charge/discharge (GCD), and electrochemical impedance spectroscopy (EIS) are the most used methods for evaluating the electrochemical performance of supercapacitors [34].

Chapter 2 - Materials and Methods

2.1 Materials

The chemicals used in this thesis, as well as the purity grades and sources, are listed in Table 2-1.

Table 2-1. The chemicals used for polymer synthesis and the electrode preparation

Chemicals	Grade	Supplier
Aniline	99.5%	Sigma-Aldrich
Cyclohexane	99%	Sigma-Aldrich
Sodium dodecylsulfate (SDS)	99%	Sigma-Aldrich
Pentanol	98%	Sigma-Aldrich
Hydrochloric acid	37%	Sigma-Aldrich
Ammonium persulfate	98.0%	Sigma-Aldrich
Sodium carboxymethyl cellulose (CMC)		Sigma-Aldrich
Acetylene black		Sigma-Aldrich
Benzene	98%	Sigma-Aldrich
Ethanol	98%	Sigma-Aldrich
Acetone	98%	Sigma-Aldrich
Stainless steel mesh		

2.2 Experimental section

2.2.1 Polymer synthesis

For the polymer synthesis, two different nanoreactors were used, the anionic bicontinuous nanoreactor system including Cyclohexane/SDS+n-pentanol/water to prepare 1D PANI nanofiber, and surfactant free microemulsion system, Benzene/Ethanol/water, for 3D packing PANI and its composite. To compare with polymers obtained via bicontinuous microemulsion approach, ice templated interfacial polymerization was applied to synthesize 2D PANI film. Polymers are named PANI fiber, 2D PANI, 3D PANI and PANI-AB based on their morphology and content, respectively.

2.2.2 Synthesis of 1D PANI fiber

An anionic bicontinuous microemulsion system consisting of Cyclohexane, SDS+n-pentanol and water was used for polymer preparation.
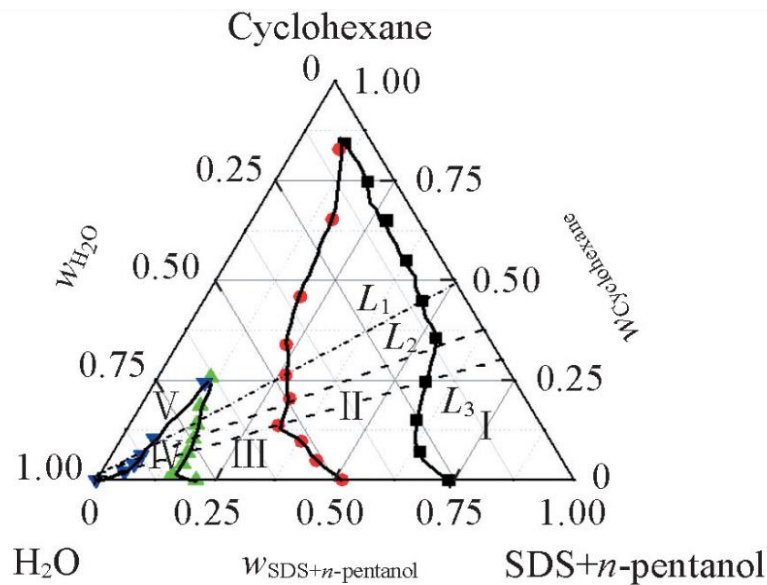
Figure 2-1. Phase diagram of an anionic bicontinuous microemulsion system [35]

In Figure 2-1, point 1 was chosen which is considered a bicontinuous area. For producing a polymer, 0.658 ml aniline monomer was dissolved in 4.61 ml cyclohexane and this solution was named A. Then 1.5 g of SDS was mixed with 2.764 ml n-pentanol, and this mixture was added to Solution A and stirred for 10 min to get cloudy dispersion. Finally, 7.5 ml ammonium persulfate (APS) solution (0.25 mol) prepared in 1M HCl was added to the monomer-containing solution and poured into a vial and left for 24 hours for complete polymerization. The received green powder was several times washed with ethanol and DI water to remove impurities.
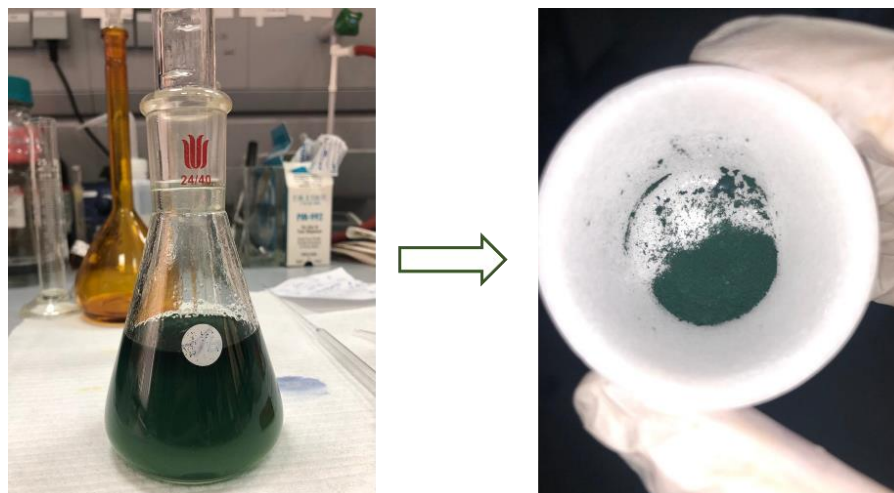
Figure 2-2. Polymerization in Cyclohexane/SDS+n-pentanol/water system and resulting product

2.2.3 Preparation of 2D PANI film

Chemical oxidative polymerization on the ice at 0°C was used to create a 2D PANI film utilizing aniline and APS as the starting materials. The water in the Petri dish was frozen at a temperature of -20°C, and the dish was flipped over to achieve a flat surface. The molar ratio of aniline to APS was 8:3, therefore 0.25 M of aniline in 1 M of hydrochloric acid and 0.25 M of APS in 1 M of hydrochloric acid were each added onto the ice surface in turn. The development of two-dimensional nanosheets with a diameter of several millimeters was apparent to the naked eye after the reaction had taken place for a period of three minutes. Following the step of transferring the PANI film to a Petri dish, the resulting polymer was subjected to several washes in deionized water and then dried in a vacuum oven for seven days. Figure 2-4 depicts the schematic representation of the formation of 2D PANI on the ice surface [36].
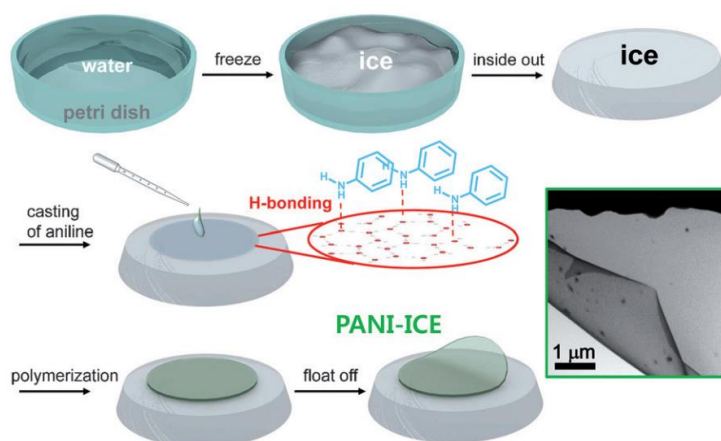
Figure 2-3. Schematic illustration of synthetic procedure on 2D PANI film [36]

2.2.4 Preparation of 3D PANI

3D PANI was synthesized using unique crosslinking agent synthesized in RESMS laboratory.

2.2.4.1 Crosslinking agent synthesis

(i) Synthesis of N-(2-hydroxyphenyl) acetamide: To a mixture of 2-aminophenol (8.34 g, 76 mmol) and THF (60 ml), acetic anhydride (8 mL) was added dropwise to a light brown solid while keeping the temperature below 50 °C and constantly stirring. The mixture, cooled to room temperature, was mixed with 50 ml of hexane and continuously stirred for 1 hour to precipitate. After that, the resulting product was filtered and washed with hexane (50 ml × 2). The solid was left overnight to dry and obtain a white crystalline powder.

Synthesis of 2-acetyl aminophenol. N-(2-hydroxyphenyl) acetamide (5 g, 33.1 mmol) and anhydrous K_2CO_3 (6.862 g, 49.65 mmol) were placed into a 100 mL round-bottom flask with 60 ml acetonitrile and stirred for 30 min at room temperature. Then dialkylhalide with carbon length of C6 (0,5 mmol eq.) was added dropwise to the mixture and refluxed for 16 h. After the reaction was finished, the solvent was removed by evaporating it at a lower pressure while also being washed out with DI water. The sediment was named Compound-2 and left overnight.
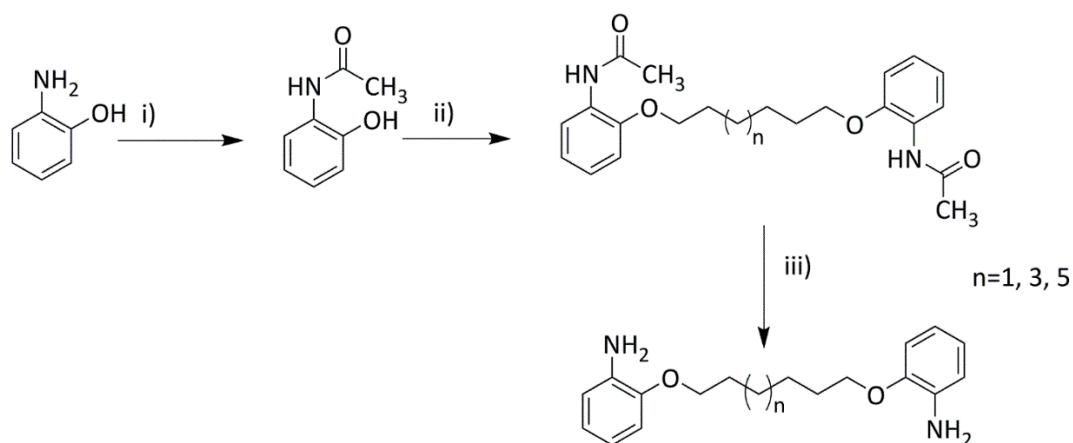
Figure 2-4. Synthesis procedure of aniline linker

(iii) Synthesis of a 2-alkoxybenzenamine. Compound-2 (9.1 g, 11 g, 5 g) was dissolved in 40 ml ethanol, and a solution of KOH (16 g, 26 g, 15 g) in 60-75 ml ethanol was added, continuously stirred, and heated at 90°C for 21 h. After that, the solvent was evaporated under reduced pressure, and diluted in water. The product then was extracted from an aqueous layer with DCM (100 mL x 2). The combined organic layers were dried with MgSO₄. Finally the solvent was evaporated under reduced pressure to give the final product.
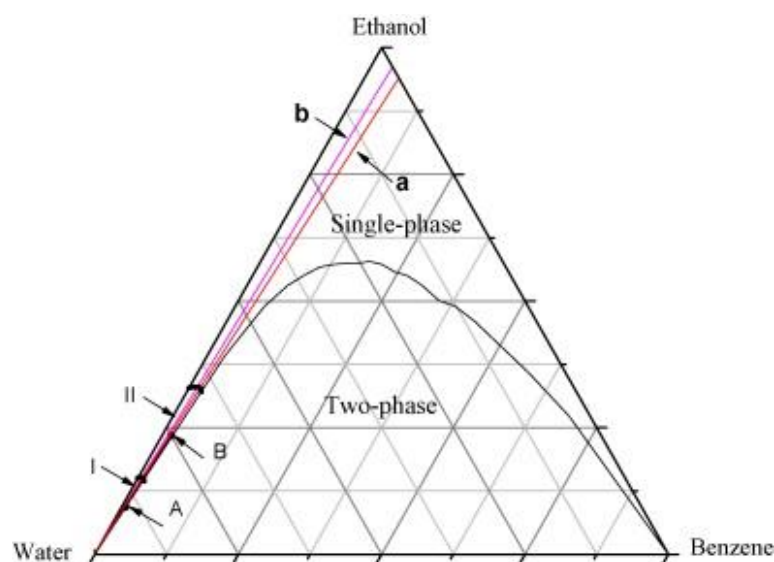
Figure 2-5. The phase diagram for the system consists of benzene/ethanol/water. The water-in-benzene area and the bicontinuous microemulsion zone are each denoted by the designations I and II, respectively [37]

2.2.4.2 3D PANI synthesis

3D PANI was synthesized using a bicontinuous microregion of a surfactant-free microemulsion system of benzene, ethanol and water [37] shown in Figure 2-6. To do this, the previously synthesized LC6 linker was mixed with aniline in a ratio of 1:200, and the resulting mixture was dissolved in benzene in a weight ratio of 20:80%. After that, APS was dissolved in 1 M hydrochloric acid at a concentration of 5 mg/ml. After that, the calculated amount of components was gently mixed and left for 12 hours for complete polymerization. To eliminate contaminants, the finished product was rinsed numerous times with ethanol and deionized water.
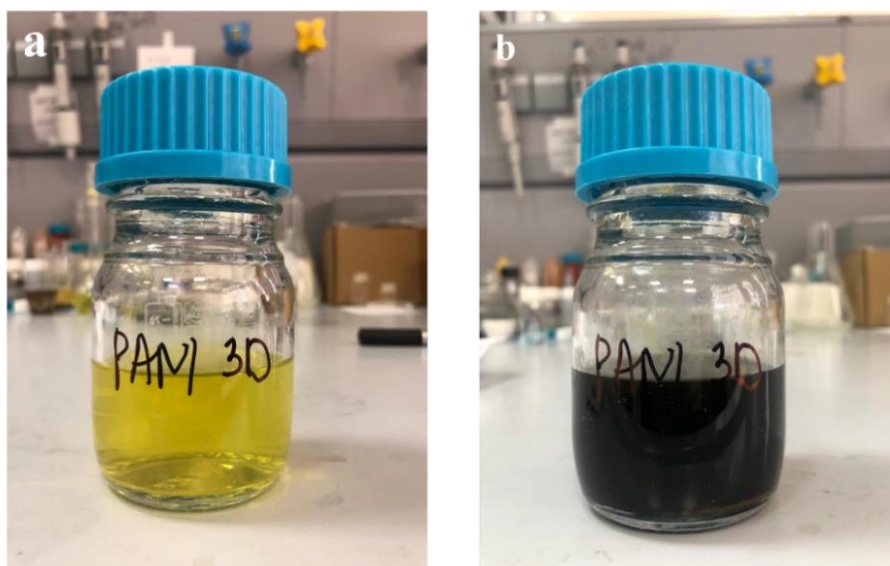
Figure 2-6. Synthesis of 3D PANI: (a) before and (b) after polymerization
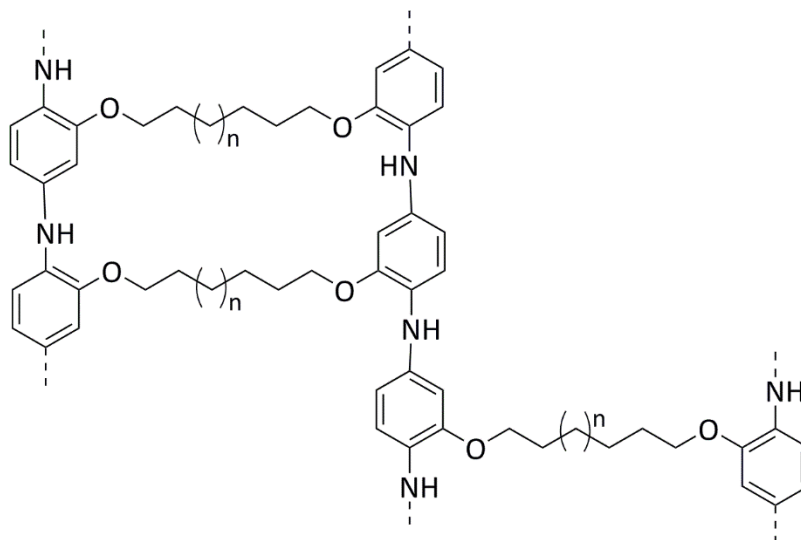
Figure 2-7. Chemical formula of crosslinked 3D polyaniline

2.2.5 Preparation of 3D PANI composite with AB

To create the PANI composite, the same experimental technique as stated in Section 2.3.4.2 was utilized [37]. Linker C6 and aniline monomer were combined at a ratio of 1:200, and the resulting mixture was dissolved in benzene at a weight% of 20:80. Acetylene black was disseminated in a 5 mg/ml APS solution in 1 M hydrochloric acid and then added to the monomer solution. The composite to monomer ratio was 1:200.
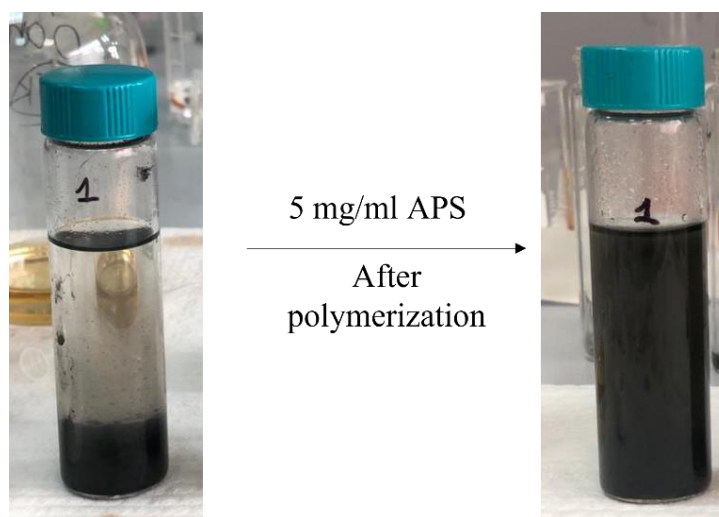
Figure 2-8. PANI AB composite polymerization

2.2.6 Electrode preparation

To make an electrode, 0.19 g of polymeric material was mixed with 0.1 g of CMC as a binder. DI water was added to the resulting mixture to obtain a suspension. The slurry was transferred to the stainless-steel mesh using blade casting method. Prepared electrodes were named PANI fiber, 3D PANI, 3D PANI-AB and placed to the vacuum oven at 60°C for 4 hours. All the prepared electrodes had a thickness of 0.15 µm.
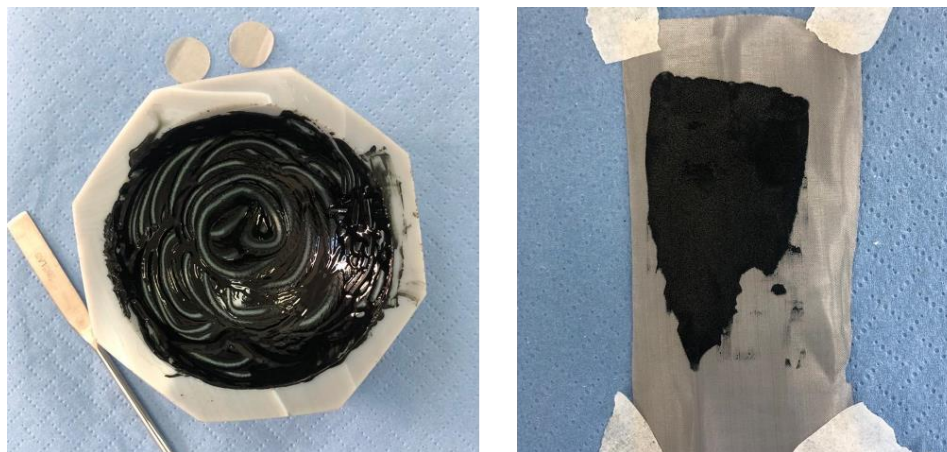
Figure 2-9. Prepared slurry and electrode of PANI fiber

2.2.7 Supercapacitor design

To assemble the supercapacitor, an H_3PO_4/PVA-based polymer gel electrolyte was initially synthesized. For this purpose, 1 g of PVA was dissolved in 9 ml of deionized water at 90 °C for two hours with magnetic stirring. After cooling the PVA solution, 1000 µl of H_3PO_4 was added and stirred for 2 hours. Using filter paper soaked with an H_3PO_4/PVA gel electrolyte and two 16 mm diameter PANI electrodes, a symmetrical split supercapacitor cell was built.

2.2.8 Materials characterization

The structure and compositional properties of the samples were characterized by FT-IR, SEM, TGA-DSC, and physical absorption of N_2, respectively. Electrochemical measurements were performed on a Bio-Logic multichannel potentiostat.

Chapter 3 - Results and Discussions

3.1 Structural and morphological analysis of the polymers

3.1.1 Structure confirmation of the polymers by FT-IR

In order to confirm structure of produced polymer FTIR spectra analysis was conducted which is depicted in Figure 3-1.
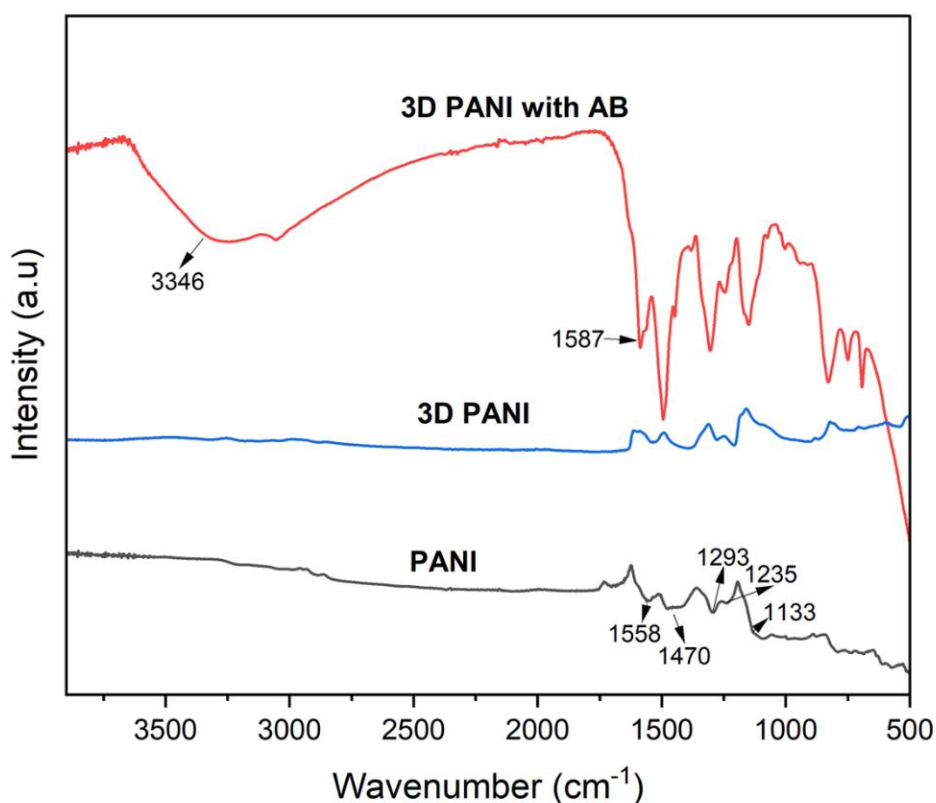
Figure 3-1. FTIR spectra of polymeric materials

The bands at 1293, 1235, and 1133 cm^{-1} are ascribed to the C–N and C–H stretching of benzenoid & quinoid rings, respectively. These absorption bands are characteristic of PANI, proving the effective synthesis of PANI [38].

The FTIR analysis of acetylene black revealed a broad absorption region at approximately 3346 cm^{-1}, which can be attributed to O-H bending vibration of hydroxyl groups. In furthermore, acetylene black displayed a prominent peak at approximately 1587 cm^{-1}, which corresponds to the C=C bending vibration of aromatic rings.

The C=C bending of the quinonoid as well as benzenoid rings, respectively, are responsible for the apparition of peaks at 1558 and 1470 cm^{-1} in PANI.

However, the shifting of the peak at 1565 cm^{-1} indicates a shift in the quinoid-to-benzenoid fraction of the polymer. This may be caused by the relationship for both polyaniline & acetylene black, which altered the polymer's oxidation state. Moreover, the composite exhibited a broad peak at approximately 3346 cm^{-1}, similar to that of acetylene black, which indicates the existence of hydroxyl groups in the acetylene black nanoparticles in the mixture.

3.1.2 Morphological characterization

The scanning electron microscope (SEM) was used to examine the surface morphology of the newly synthesized polymeric materials at 5 kV and 200 pA. The shape of a PANI nanofiber is depicted here in Figure 3-2. The nanofibers have a diameter of an average of 130 nm and are consistent over the entire sample, as the figure clearly demonstrates. In addition, the surface of nanofibers is highly gritty and rough in appearance. The crystallization of oxidized organic molecules might be to account for this phenomenon.
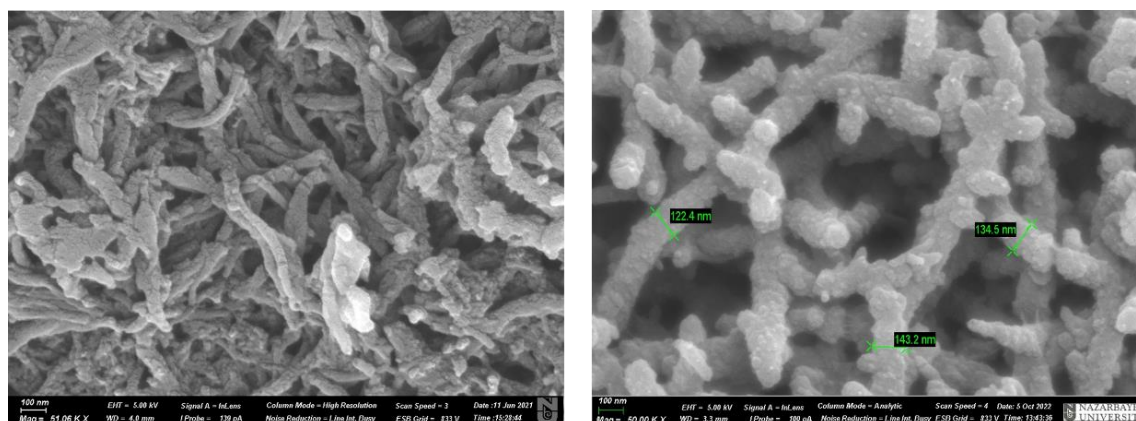
Figure 3-2. SEM image of PANI fiber

A polyaniline film with a thickness of 200 nm was produced as a result of polymerization carried out on ice. The coating is extremely porous and relatively thin, as can be seen in Figure 3–3. These structure is due to the high concentration of the oxidant, which causes the creation of a large number of nucleation centers. Moreover, the film has a different surface structure on both sides. One surface that was on the ice is smooth, while the other is rough. As in the case of polyaniline nanofibers, surface roughness can be associated with the crystallization of oxidized organic molecules [29].
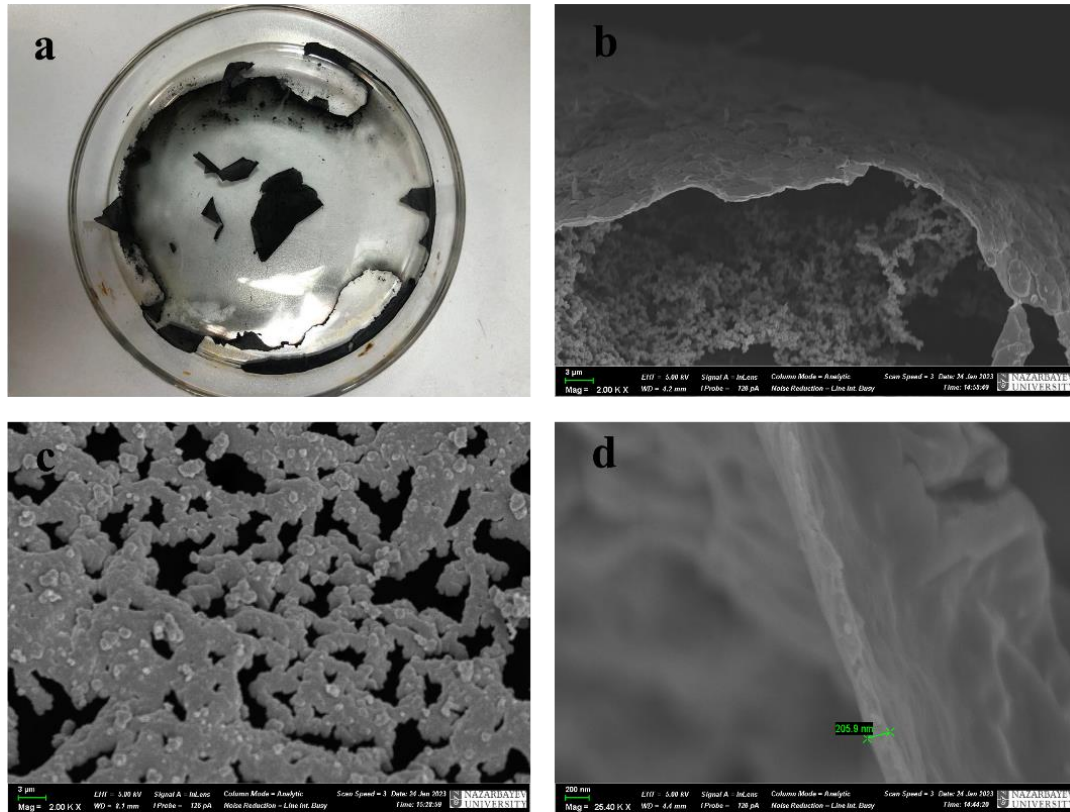
Figure 3-3. Synthesized PANI film (a) and its SEM image at 1 μm (b), 3 μm (c) and 300 nm

3D polyaniline has a loose, porous structure like a sponge. Nanoparticles are short, and fibrous. Between the fibers, clearly seen the pores formed as a result of tailoring with the linker. However, zooming in and determine the particle size was impossible due to the low electrical conductivity of the polymer.
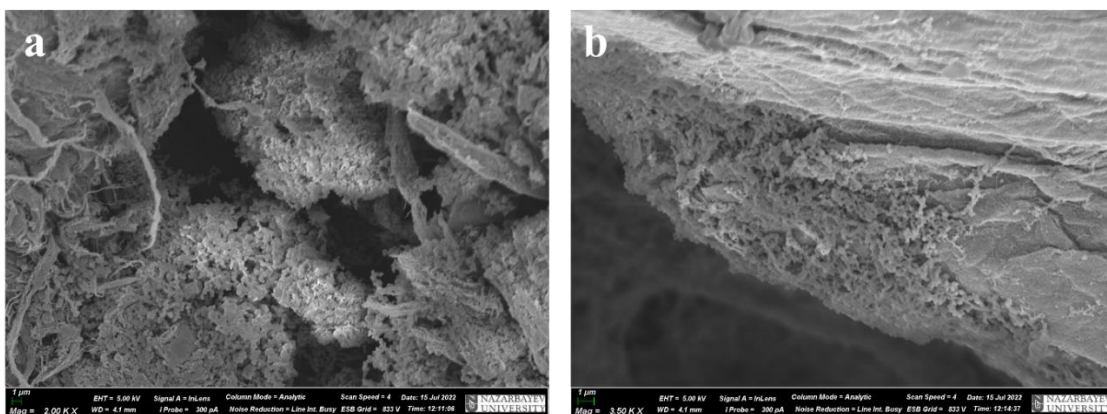
Figure 3-4. Surface morphology (a) and cross-section (b) of 3D PANI

Figure 3-5 depicts the resulting 3D PANI-AB composite and its surface morphology. As in the case of 3D PANI, the composite has a spongy porous structure due to the presence

of a crosslinking agent. As shown in Figure 3-5b, the AB additive is placed in the pores that are created between the aniline particles that look like small fibers. Moreover, it can be said that the filler is evenly distributed over the entire surface of the sample.
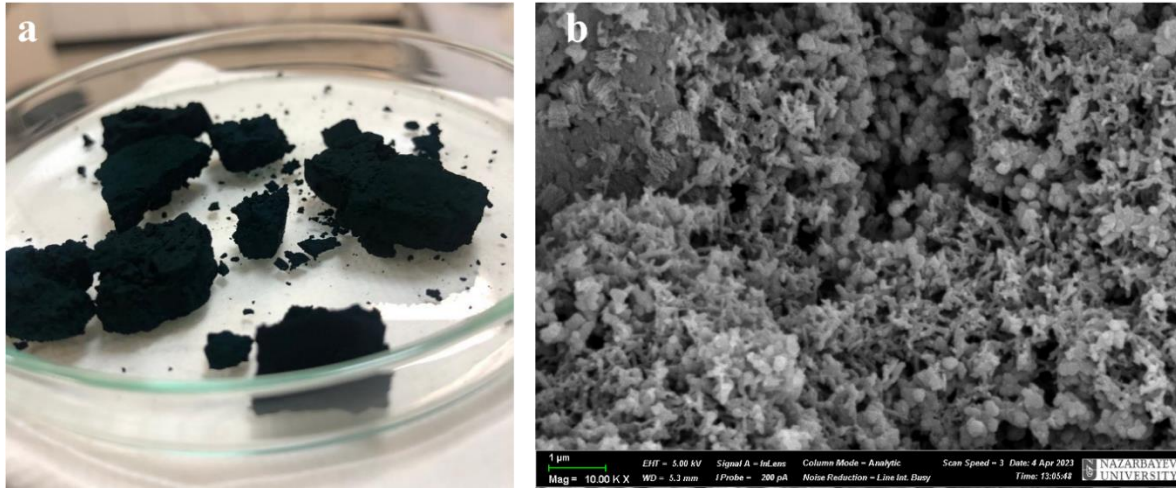
Figure 3-5. (a) PANI AB composite and its SEM image (b)

3.1 Thermal stability
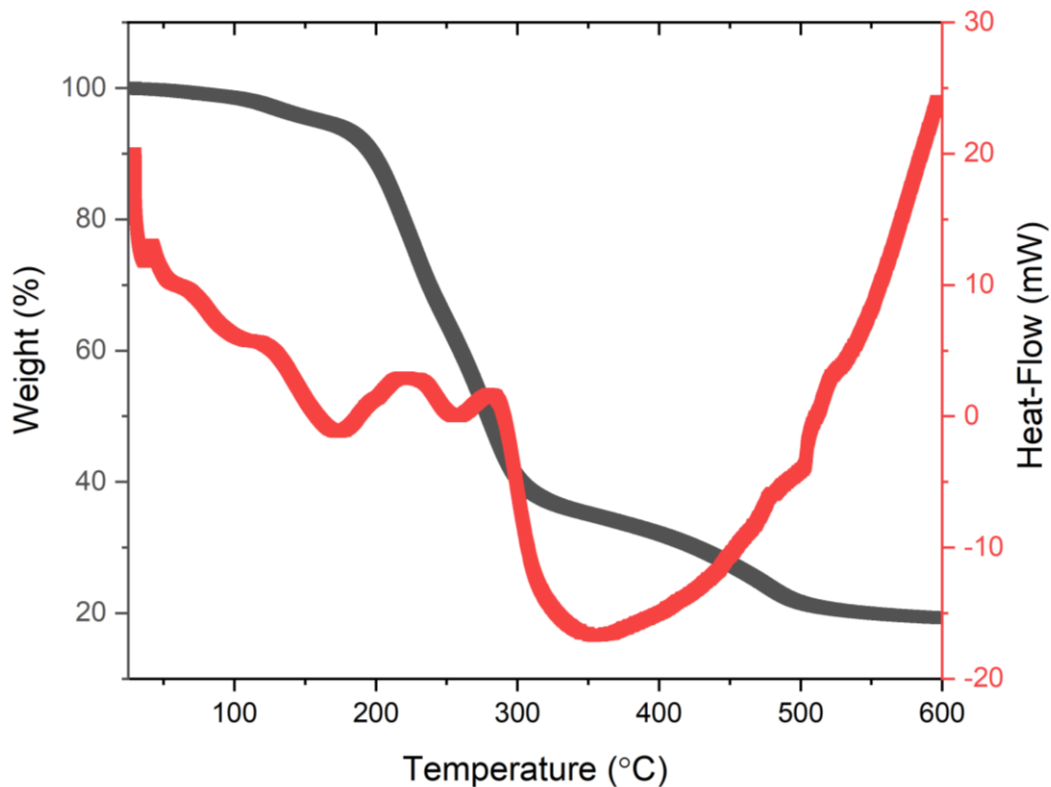
Figure 3-6. TGA-DSC curves of PANI fiber at 10°C min⁻¹ under nitrogen atmosphere

Figure 3-6 depicts the TG-DSC curves of the PANI fiber. All polyanilines exhibited similar two-step mass loss processes, consistent with other observations. The thermogram indicated that decomposition began at 171 °C, with most of the weight loss occurring around 180 and 500 °C. Around 50 to 130 °C, water and dopant materials were expelled from the polyaniline matrix, which led to the initial weight loss. The second step takes place at approximately 450°C, when the material endures the majority of its degradation and creates stable products such as carbon and nitrogen oxides. Polyaniline has a high thermal stability and can endure high temperatures without degrading. [39], [40]

On the DSC plot of PANI fiber, one curve difference and three endotherms are readily discernible. The first endotherm begins at approximately 41°C and ends at approximately 69°C, which corresponds to the temperature of the glass transition (T_g). The second endotherm begins at approximately 75°C and ends at approximately 123°C with a broad peak at approximately 98°C, followed by the third endotherm, which begins at approximately 126°C and ends at approximately 215°C with a peak at approximately 173°C. And the fourth endotherm, which begins at approximately 226°C and ends at approximately 283°C with a maximum at approximately 259°C matching to a melting temperature (T_m). The fifth endotherm, which begins at approximately 279 °C and ends at approximately 478°C.

The number and location of these endothermic maxima can be affected by a variety of variables, including the method of synthesis, molar mass, crystallinity level, and type of dopant [41]– [44].

In certain instances, PANI may exhibit extra endothermic peaks owing to other thermal transitions, such as dehydration or solvent desorption.

3.1.4 Specific surface area measurement

Considering the capacitive behavior of polymer supercapacitors based on reactions occurring at the electrode surface, the surface area of the electrode material is crucial determinant of the quantity of active material accessible to redox reactions.

The BET surface of the materials are 30 m^2/g, 10 m^2/g, 27.7 m^2/g, and 19.5 m^2/g for PANI fiber, 2D PANI, 3D PANI and 3D PANI-AB composite, respectively. From the isotherms shown in Figure 3-7, can be observed that the amount of the adsorbed nitrogen is in this order 38.7 cm^3/g for PANI fiber > 30.74 cm^3/g for 3D PANI > 19.53 cm^3/g for 3D

PANI-AB composite > 15.2 cm³/g for 2D PANI film.
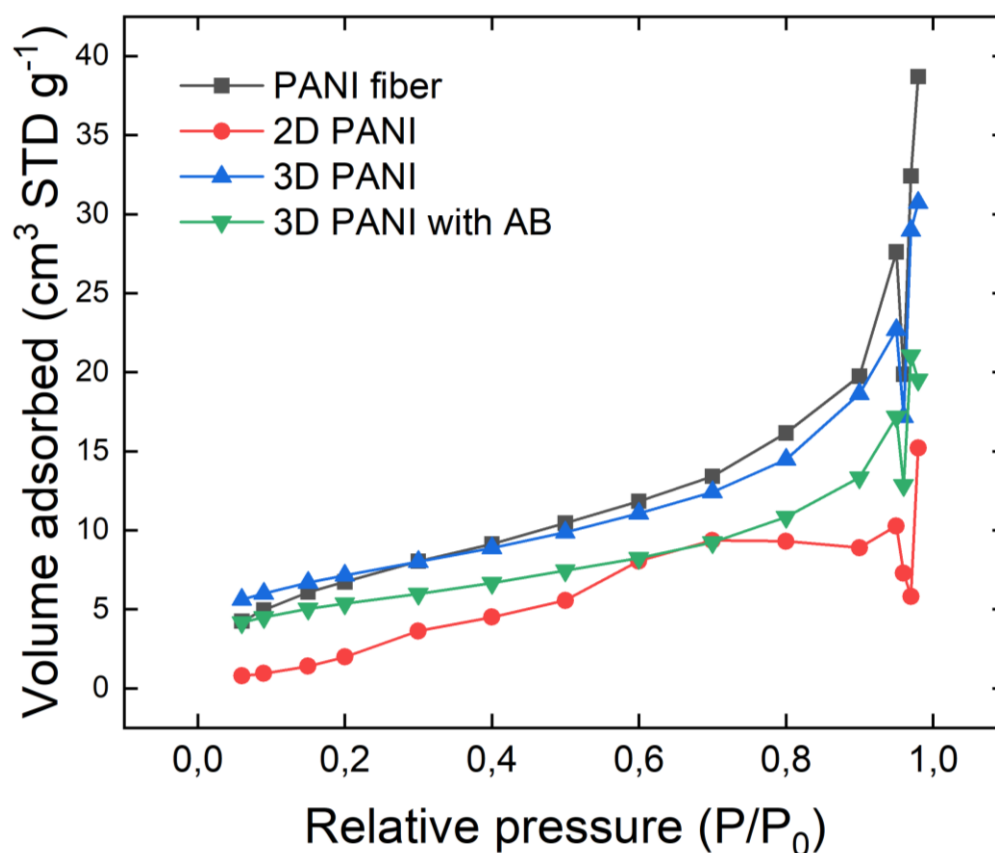
Figure 3-7. The nitrogen adsorption isotherms of polymeric materials

By comparing the results, it is found that the PANI fiber has high surface are owing its relatively long and thin morphology. Because of the presence of the crosslinking agent, 3D PANI also has a good surface area [45]. This characteristic of the polymer can be improved by increasing the concentration of the linker. As for the composite, its small surface area can be explained by the presence of AB, which, according to the literature data, has a specific surface area of 16–64 m^2 g^{-1}. During the polymerization of AB with aniline monomer, a covalent bond is formed between the two components. Hence, the AB adheres tightly to the polymer and thus covers the pores [46].

3.2 Electrochemical performance evaluation

3.2.1 Electrochemical Impedance spectroscopy

Figure 3-8 depicts the Nyquist plot of the electrodes in different frequency ranges

based on the nature and properties of the polymeric material. For PANI fiber, 3D PANI and PANI AB impedance (Figure 3-6 a, c, d) was obtained in range from 10^5 Hz to 0.01 Hz, while for 2D film it was observed in range from 10^6 Hz to 0.01 Hz.

Calculations were made to determine the internal resistance of the polymeric materials by using the X-intercept found in the high-frequency area of the Nyquist plot. The computed values of the internal resistance for PANI fiber are 4,48 Ω, whereas the values for 3D PANI and 3D PANI-AB composite are 22,4 and 16,8 Ω, respectively. The obtained internal resistance data was further used to calculate the electrical conductivity of materials according to Equation 1 [47]:

$$\sigma = \frac{1}{R_S} \times \frac{L}{A} \tag{1}$$

where R_S – is internal resistance of material, A – area of the electrode. The results of the conductivity calculations are $2.2 \times 10^{-4}\ S\ cm^{-1}, 4.3 \times 10^{-5}\ S\ cm^{-1},$ and $5.7 \times 10^{-5}S\ cm^{-1}$ for PANI fiber, 3D PANI and PANI-AB, respectively.
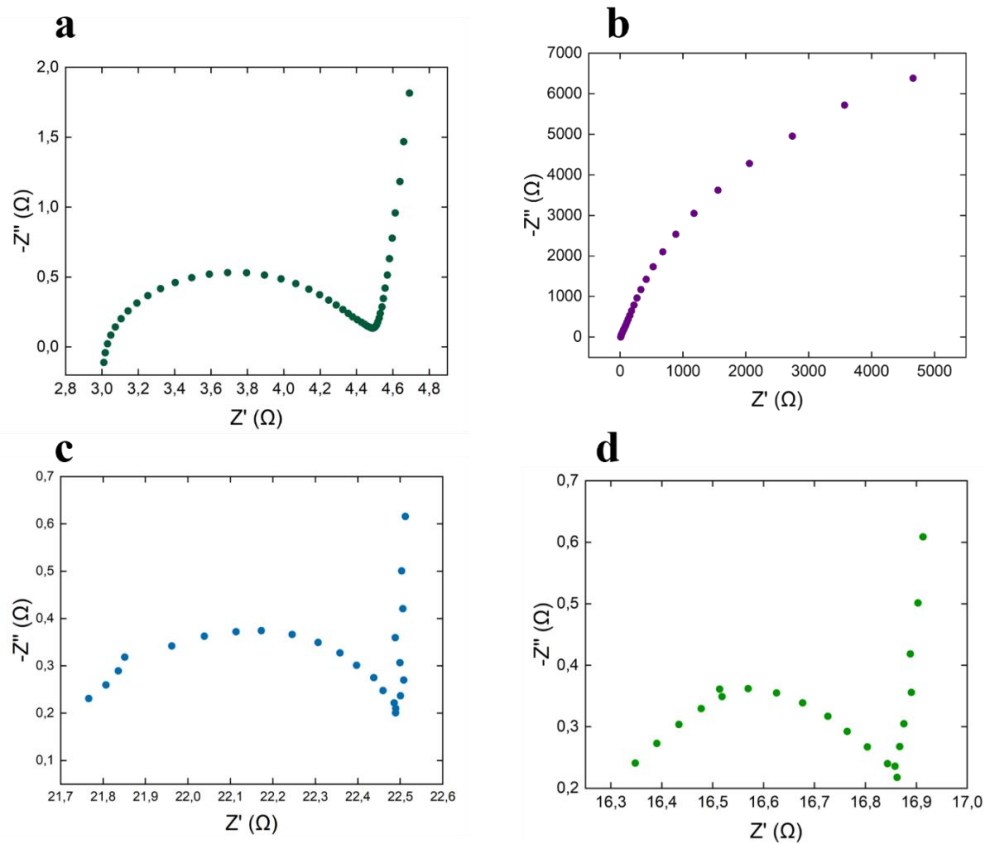

Figure 3-8. Nyquist plot of PANI fiber (a), 2D PANI film (b), 3D packed PANI (c) and PANI-AB composite (d)

By comparing the results obtained for PANI fiber, 3D PANI and 3D PANI composite with AB, found that 3D PANI has a higher internal resistance which is owing to its crosslinked 3D network structure generating a significant number of electron pathways. Moreover, owing to these paths being neither continuous nor straight, electrons encounter resistance as they pass through the substance. This resistance is exacerbated by the fact that the crosslinked structure restricts the mobility of the electrons, making it difficult for them to freely move through the material.

During the polymerization process, π-π interaction may have been formed between the acetylene black surface and the aniline monomers, which may explain why the PANI-AB composite has a higher conductivity. The creation of the connections between the filler and the polymer may increase interfacial adhesion between the two materials, which ultimately results in improvements to the composite material's mechanical and electrical characteristics. Additionally, the formed interaction prevents the AB particles from agglomeration and ensures their even distribution, both of which contribute to an increase in the material's electrical conductivity [47].

The conductivity of a supercapacitor's electrode material is a critical parameter that determines the rate at which it can be charged and discharged, as well as its overall energy storage capacity. Hence, the results of cyclic voltammetry and the charge-discharge curve can be analyzed based on it [48].

Figure 3-2b denotes the Nyquist plot of 2D PANI film which has no semicircle in high frequency region. Moreover, the resistance of the diffusion layer is high enough. It demonstrates the absence of capacitive or inductive behavior of the polymer.

3.2.2 Cyclic voltammetry

Cyclic voltammetry of the assembled supercapacitor cells was performed in a voltage window from -0.5 to 0.5 V at different scan rates.
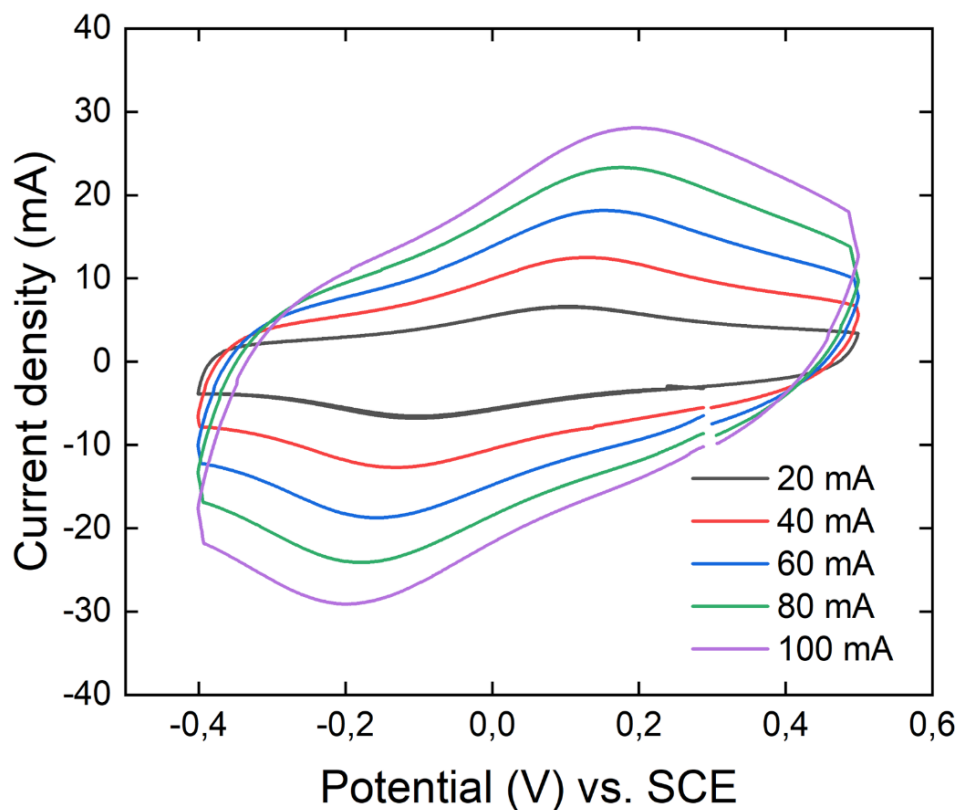
Figure 3-9. Cyclic voltammetry curve of PANI fiber at different scan rates

As illustrated in Figure 3-9, CV curve of PANI fiber has rectangular shape that the material has ability to store charge electrostatically with no contribution from Faradaic process. Moreover, two pairs of redox peaks due to redox transformations owing to the conversion from fully reduced to conducting, from conducting to fully oxidized states, leucoemeraldine to emeraldine and emeraldine to pernigraniline, respectively (Scheme 3-1). It should be noted that these reactions are reversible, and their characteristic peaks are responsible for the pseudocapacitive behavior of PANI [29].
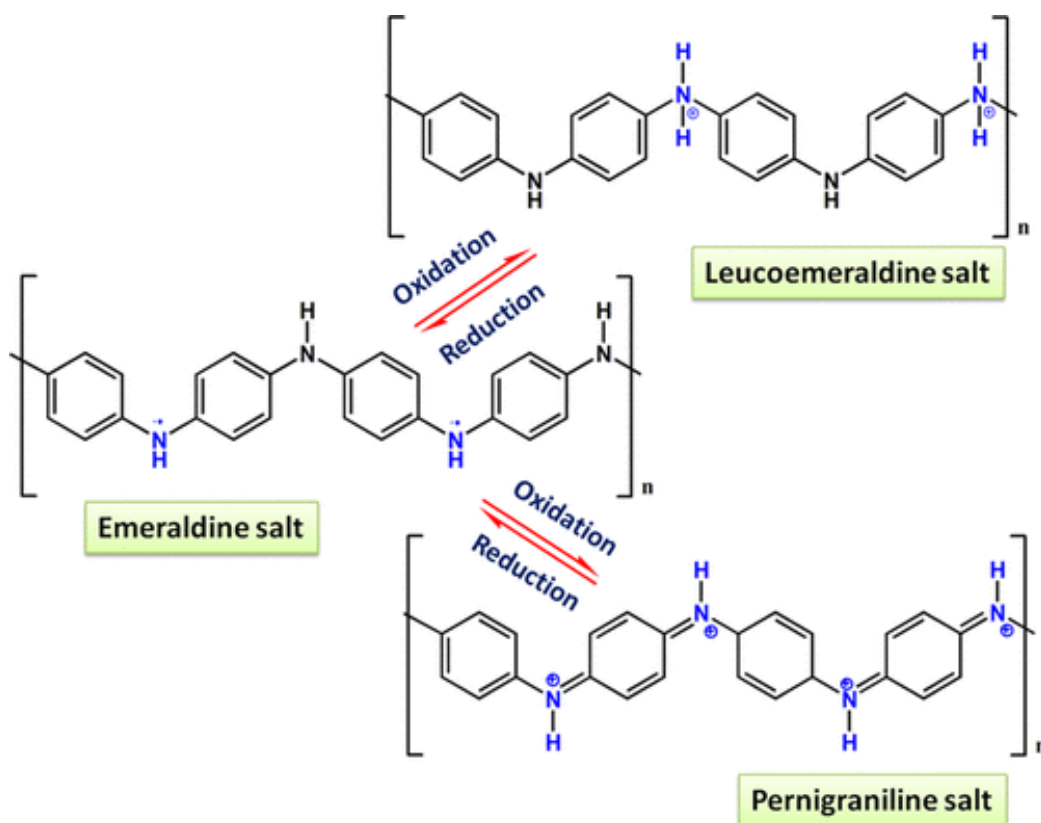
Scheme 3-1. Structural conversion of PANI [29]

In Figure 3-10 shown cyclic voltammetry curve of 2D PANI. As can be seen from the figure, 2D film has no capacitance because of the very small specific surface area [49]. Moreover, based on the EIS results it can be concluded that there is no ion transfer which leads to the lack of capacitive behavior. Thus, based on this information the supercapacitor designed using 2D PANI thin film was not considered further.
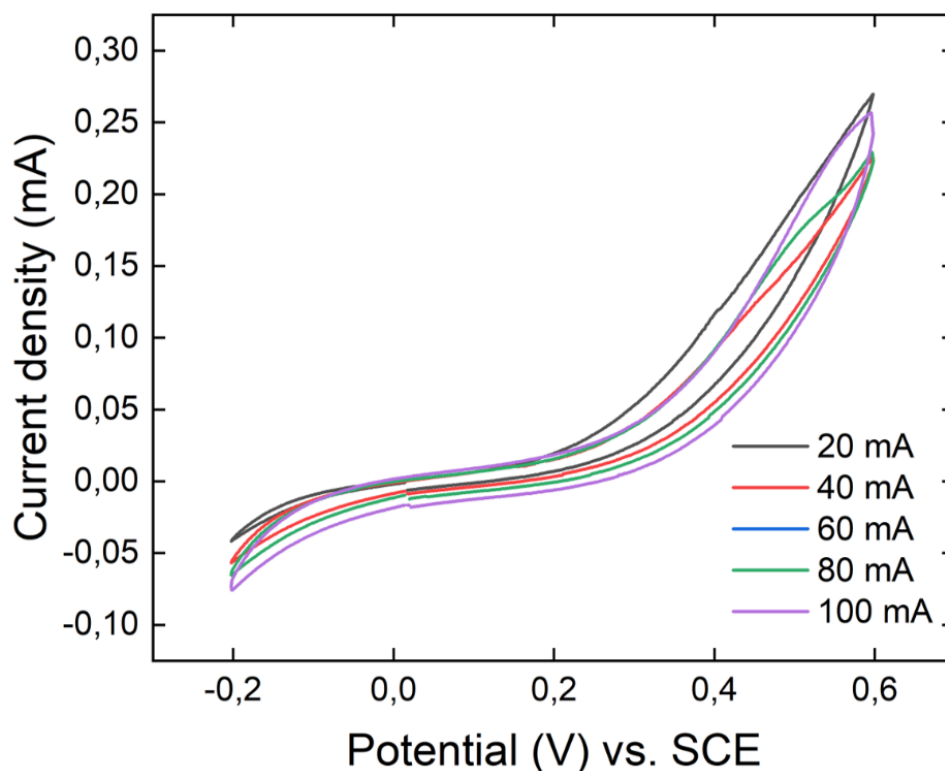
Figure 3-10. Cyclic voltammetry curve of 2D PANI film at different scan rates

As seen from Figure 3-11, the cyclic voltammetry curve of 3D PANI has a rectangular shape, where no redox peaks observed. This phenomenon is associated with a higher degree of disorder compared to the PANI fiber, which prevents the formation of stable redox states of the polymer. The rectangular shape of the curve related to the good surface area of 3D PANI (See Section 3.1.4) which generates more active sites for electrochemical reactions [49], [50].

However, due to the low conductivity of the polymer, CV curve of 3D PANI has a less steep slope than in the case of PANI fiber. The low conductivity leads to an increase in internal resistance, this can decay the overall performance of the supercapacitor and affect to its energy storage capacity.
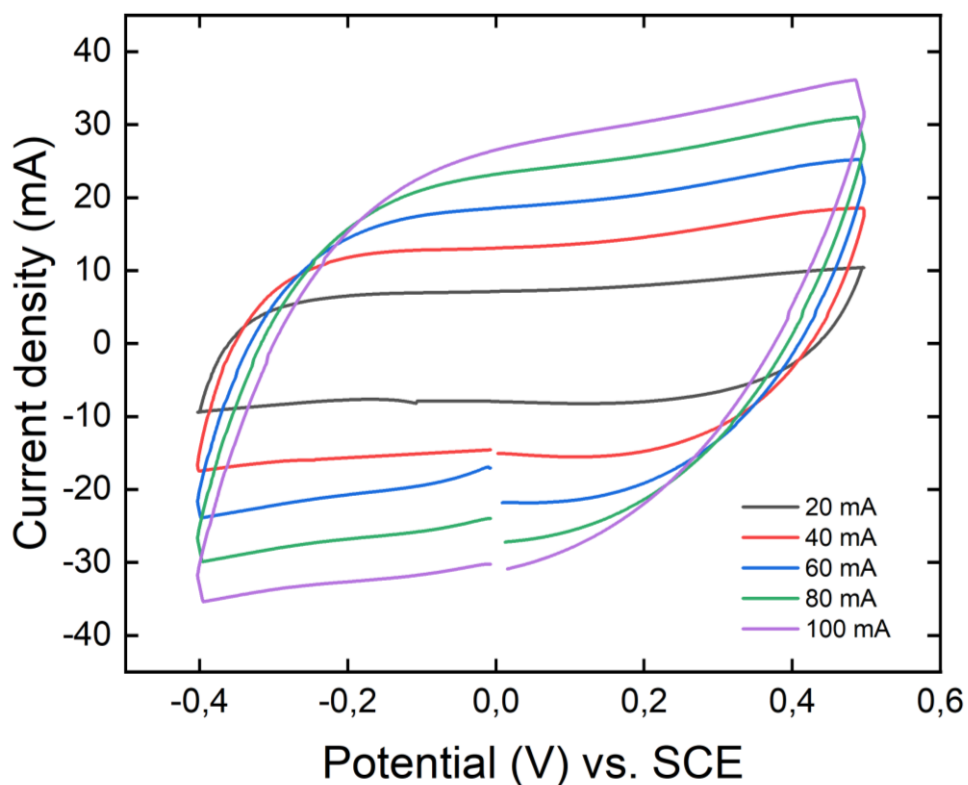
Figure 3-11. CV curves of 3D PANI at different scan rates

Compared with 3D PANI, the 3D PANI-AB composite has a non-rectangular CV curve with a shallow slope (Figure 3-12). Despite the fact that the material has higher conductivity, its small surface area limits the amount of charge that can be stored through redox reactions that happen on the surface [49].
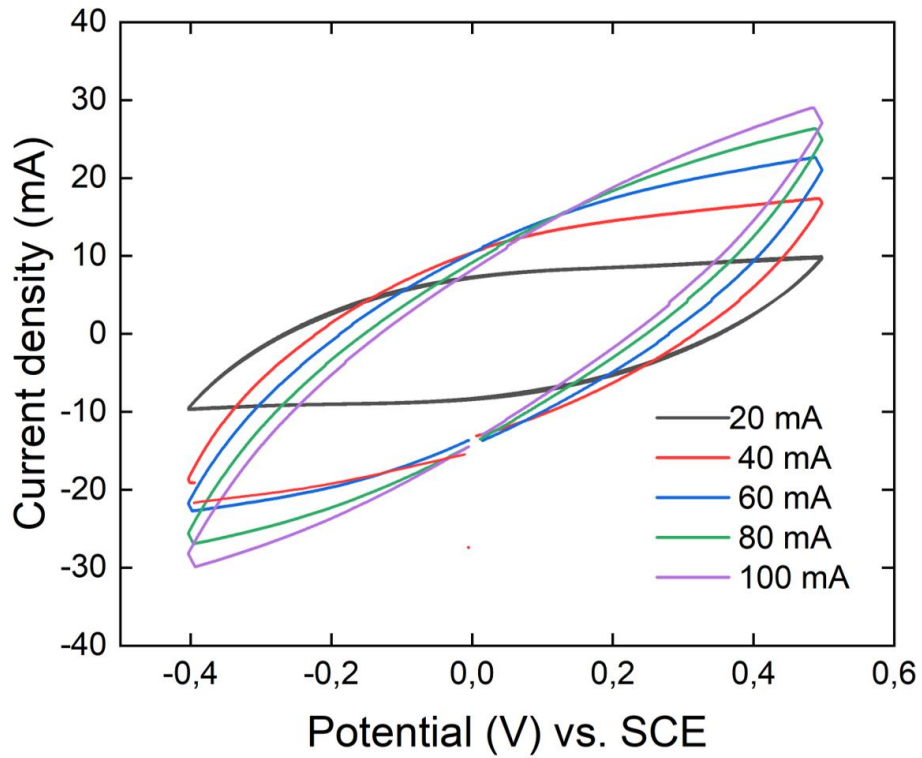
Figure 3-12. CV curve of 3D PANI composite with AB at different scan rates

3.2.3 Galvanostatic charge-discharge analysis

Figure 3-13, 3-14 display the GCD curves of PANI fiber and 3D PANI at current density of 1 mA, respectively.
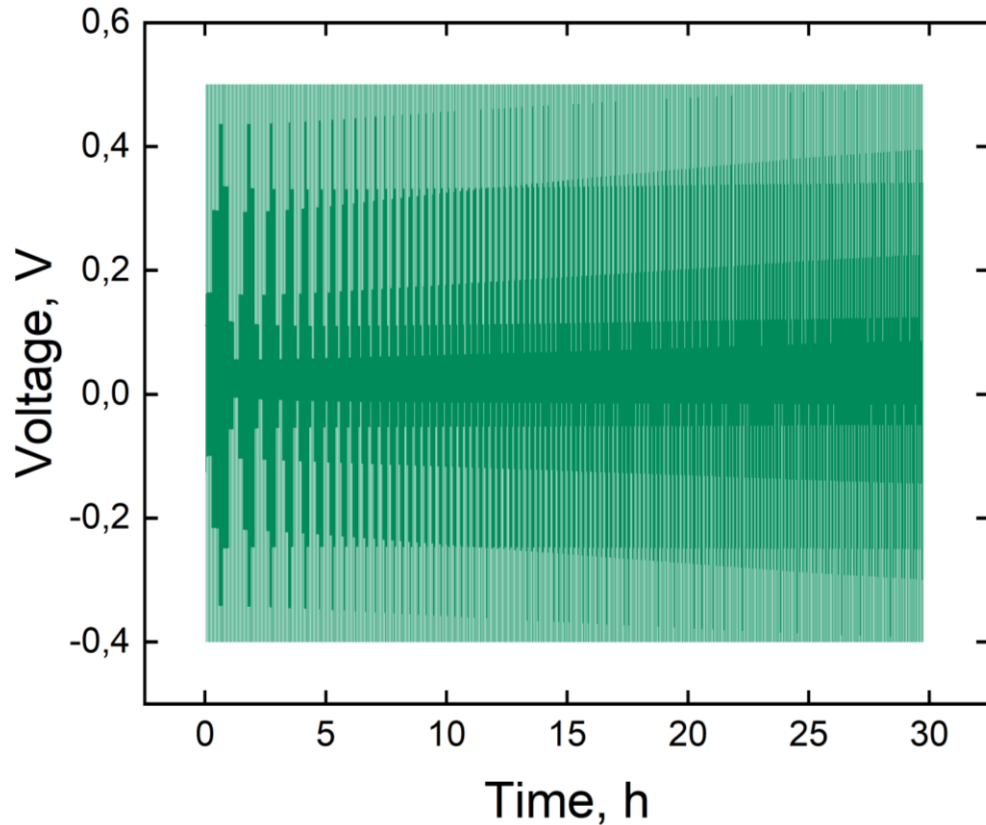
Figure 3-13. GCD curve of PANI fiber at current density of 1 mA.

As was determined from the GCD curve PANI fiber has 1000 cycles in 30 hours, while 3D PANI has only 637 cycles in 41 hours which indicate that the first material has higher cycle life, but the second one has higher cycle rate.

Cycle life is the number of charge-discharge cycles a supercapacitor can endure before its performance substantially degrades. An extended lifetime indicates that the performance of the supercapacitor can be maintained for a longer period of time. In this instance, the PANI fiber supercapacitor has a longer lifespan of 1000 cycles compared to the 3D PANI supercapacitor's 637 cycles.

In contrast, cycle rate refers to the rate at which a supercapacitor can undergo charge-discharge cycles. This indicates that the supercapacitor can charge and discharge more rapidly. The 3D PANI supercapacitor has a cycle rate of approximately 15.5 cycles per hour, whereas the PANI fiber supercapacitor has a cycle rate of approximately 33.3 cycles per hour.
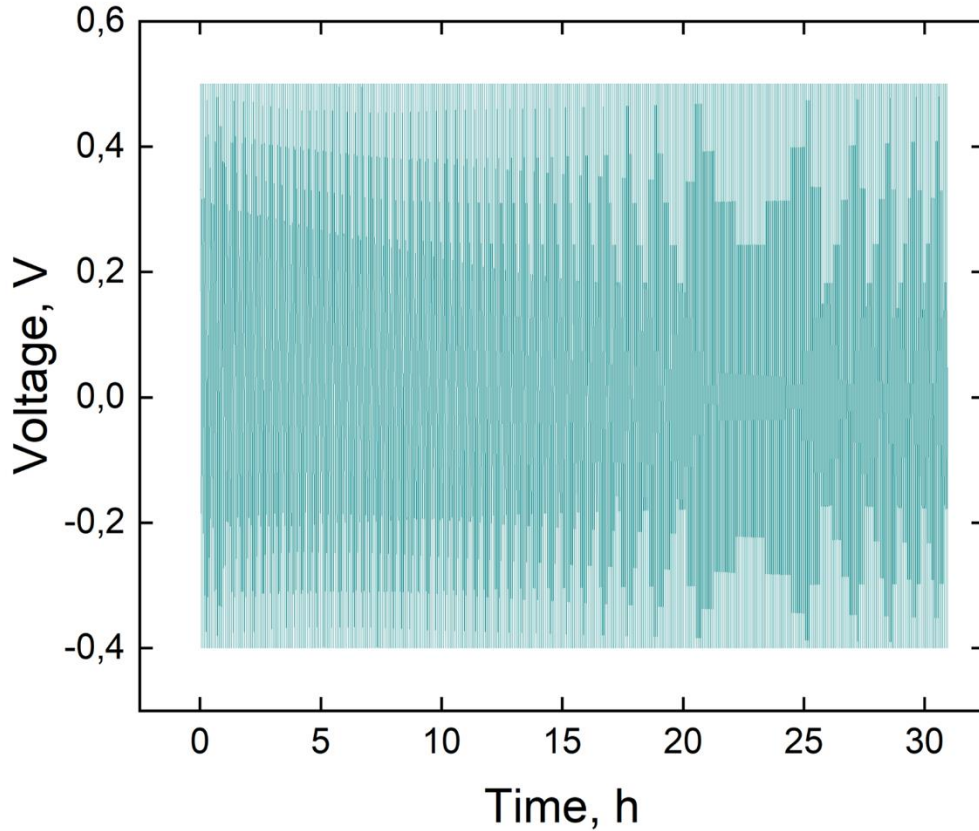
Figure 3-14. GCD curve of 3D PANI at current density of 1 mA.

From the GCD curve specific capacitance of the electrodes were calculated using Equation 2:

$$C_S = \frac{I \times \Delta t}{\Delta V \times m} \qquad (2)$$

where I is the constant current in A applied in the charge–discharge process, Δt is the discharge time in s, m is the mass of the active material in g, and ΔV is the voltage window in charge–discharge experiments in V [29].

Moreover, using Equation 3 and Equation 4 energy and power density of the cells are calculated.

$$E = \frac{C_S \Delta V^2}{2 \times 3600} \qquad (3)$$

$$P = \frac{E \times 3600}{\Delta t} \qquad (4)$$

where I is the constant current in A applied in the charge–discharge process, Δt is the discharge time in s, m is the mass of the active material in g, and ΔV is the voltage window in charge–

discharge experiments in V [29]. Energy and power densities if the polymer based supercapacitors are 14.02 W h g^{-1} and 900 μW h g^{-1} for PANI fiber and 2.9 W h g^{-1} and 183 μW h g^{-1}.

According to the specific capacitance equation calculated from the charge-discharge curve, the specific capacitance values of PANI and 3D PANI fibers at a current density of 1 A g–1 are 280.4 and 58.8 F g–1, respectively. The low specific capacitance of 3D PANI is due to its relatively small surface area and electrical conductivity.
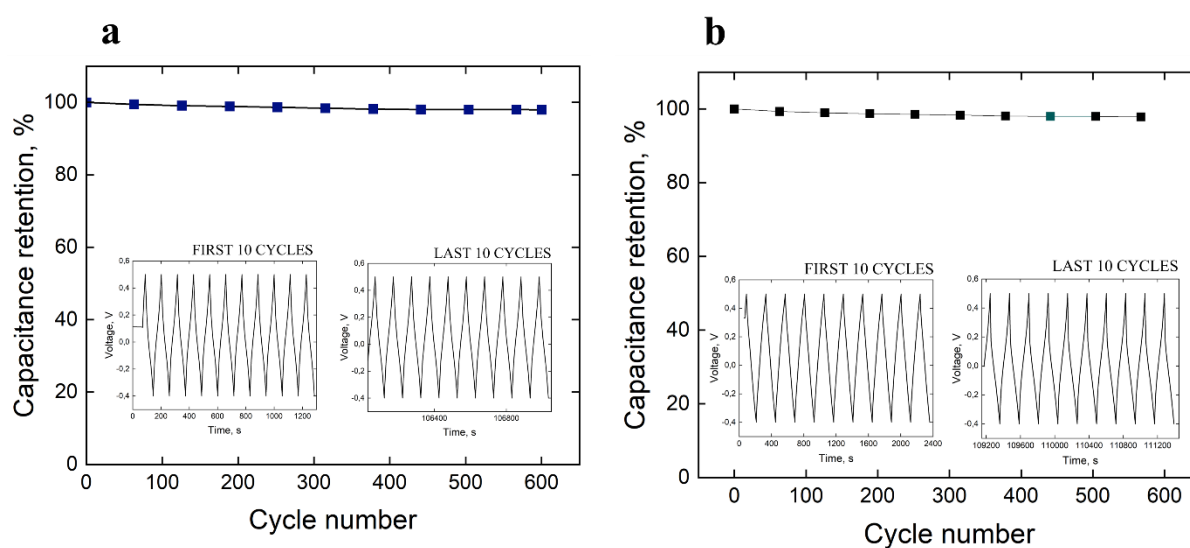
Fiber 3-15. Cycle life test of (a) PANI fiber and (b) 3D PANI symmetric supercapacitor cell

Figure 3-15 summarizes the specific capacitance of assembled symmetric cell of PANI fiber and 3D PANI. As can be seen form Figure, supercapacitor cells have initial capacitance of 280.4 F g^{-1} for PANI fiber and 58.85 F g^{-1} for 3D PANI. However, they lost their capacitance on the first 200 cycles. This phenomenon can be associated with initial surface activation. The first cycles may be required to activate the electrode surface and establish a stable electrochemical interface between the electrode and the electrolyte. Once surface is fully activated, the electrodes stabilized.

Conclusion

In summary, this work presents a simple method of bicontinuous microemulsion polymerization, thanks to which it was possible to synthesize both 1D PANI nanofibers and 3D cross-linked architecture and its composite. Moreover, a 2D polyaniline film was also presented to compare the effect of morphology on the electrochemical properties of materials. To confirm the formation of the abovementioned polymer materials structural and morphological analysis were conducted. Moreover, capacitive behavior of designed symmetric cells was also investigated utilizing EIS, CV and GCD tests.

The PANI nanofibers obtained as a result of the study show the best electrochemical properties among all synthesized materials, while it was found that the 2D film does not have the properties required for supercapacitors.

FTIR and TGA confirmed the successful synthesis of PANI nanofibers. The morphology study also confirms that PANI nanofibers do indeed have a nanoform. PANI nanofibers have a specific capacitance of 280.4 F g^{-1} at a current density of 1 A g^{-1} and good cyclic stability of 98% up to 1000 cycles. Moreover, this electroactive material showed good specific power and specific energy, which are equal to 900 μW h g^{-1} and 14.02 W h g^{-1}, respectively. These results are explained by and subject to its relatively large surface area and electrical conductivity.

On the other hand, it was found from the charge-discharge curves that 3D PANI also tends to rapidly charge and discharge, which shows how quickly a supercapacitor can store and release energy. However, the composite material obtained on the basis of 3D PANI with AB had rather poor electrochemical characteristics due to its small surface area.

The use of polymeric materials for energy storage is a promising direction. Although the electrochemical characteristics of the polymers obtained in this research work can be considered quite good, they still need some improvement. I think the main problem is not enough surface area. To do this, I need to synthesize crosslinkers with different lengths of carbon atoms that can increase the surface area of the material without obviously affecting its conductivity. Moreover, I need to test different fillers for the polymer, in order to reduce its internal resistance.

References

[1] F. A. Permatasari, M. A. Irham, S. Z. Bisri, and F. Iskandar, "Carbon-based quantum dots for supercapacitors: Recent advances and future challenges," *Nanomaterials*, vol. 11, no. 1. MDPI AG, pp. 1–34, Jan. 01, 2021. doi: 10.3390/nano11010091.

[2] D. Chen, Q. Wang, R. Wang, and G. Shen, "Ternary oxide nanostructured materials for supercapacitors: a review," *J Mater Chem A Mater*, vol. 3, no. 19, pp. 10158–10173, 2015, doi: 10.1039/C4TA06923D.

[3] A. H. Siddique, R. Butt, S. W. Bokhari, D. V. Raj, X. Zhou, and Z. Liu, "All graphene electrode for high-performance asymmetric supercapacitor," *Int J Energy Res*, vol. 44, no. 2, pp. 1244–1255, Feb. 2020, doi: 10.1002/er.4893.

[4] W. Raza *et al.*, "Recent advancements in supercapacitor technology," *Nano Energy*, vol. 52, pp. 441–473, Oct. 2018, doi: 10.1016/j.nanoen.2018.08.013.

[5] S. Huang, X. Zhu, S. Sarkar, and Y. Zhao, "Challenges and opportunities for supercapacitors," *APL Mater*, vol. 7, no. 10, p. 100901, Oct. 2019, doi: 10.1063/1.5116146.

[6] H. Lv, Q. Pan, Y. Song, X.-X. Liu, and T. Liu, "A Review on Nano-/Microstructured Materials Constructed by Electrochemical Technologies for Supercapacitors," *Nanomicro Lett*, vol. 12, no. 1, p. 118, Dec. 2020, doi: 10.1007/s40820-020-00451-z.

[7] Poonam, K. Sharma, A. Arora, and S. K. Tripathi, "Review of supercapacitors: Materials and devices," *J Energy Storage*, vol. 21, pp. 801–825, Feb. 2019, doi: 10.1016/j.est.2019.01.010.

[8] Y. Shao *et al.*, "Design and Mechanisms of Asymmetric Supercapacitors," *Chem Rev*, vol. 118, no. 18, pp. 9233–9280, Sep. 2018, doi: 10.1021/acs.chemrev.8b00252.

[9] S. Shiraishi, "Electric Double Layer Capacitors," in *Carbon Alloys*, Elsevier, 2003, pp. 447–457. doi: 10.1016/B978-008044163-4/50027-9.

[10] L. Zhou, C. Li, X. Liu, Y. Zhu, Y. Wu, and T. van Ree, "Metal oxides in supercapacitors," *Metal Oxides in Energy Technologies*, pp. 169–203, Jan. 2018, doi: 10.1016/B978-0-12-811167-3.00007-9.

[11] S. Shiraishi, "Electric Double Layer Capacitors," *Carbon Alloys: Novel Concepts to Develop Carbon Science and Technology*, pp. 447–457, Jan. 2003, doi: 10.1016/B978-008044163-4/50027-9.

[12] T. Funabashi, "Introduction," *Integration of Distributed Energy Resources in Power Systems: Implementation, Operation and Control*, pp. 1–14, Jan. 2016, doi: 10.1016/B978-0-12-803212-1.00001-5.

[13] P. Kurzweil, "CAPACITORS | Electrochemical Polymer Capacitors," *Encyclopedia of Electrochemical Power Sources*, pp. 679–684, Jan. 2009, doi: 10.1016/B978-044452745-5.00355-5.

[14]   G. Z. Chen, "Supercapattery: Merit-merge of capacitive and Nernstian charge storage mechanisms." [Online]. Available: https://www.nottingham.edu.cn/en/library/documents/research-

[15]   Y. Jiang and J. Liu, "Definitions of Pseudocapacitive Materials: A Brief Review," *ENERGY & ENVIRONMENTAL MATERIALS*, vol. 2, no. 1, pp. 30–37, Mar. 2019, doi: 10.1002/eem2.12028.

[16]   Y. Zhang *et al.*, "Progress of electrochemical capacitor electrode materials: A review," *Int J Hydrogen Energy*, vol. 34, no. 11, pp. 4889–4899, Jun. 2009, doi: 10.1016/j.ijhydene.2009.04.005.

[17]   A. G. Pandolfo and A. F. Hollenkamp, "Carbon properties and their role in supercapacitors," *J Power Sources*, vol. 157, no. 1, pp. 11–27, Jun. 2006, doi: 10.1016/j.jpowsour.2006.02.065.

[18]   Y. Shao *et al.*, "Design and Mechanisms of Asymmetric Supercapacitors," *Chem Rev*, vol. 118, no. 18, pp. 9233–9280, Sep. 2018, doi: 10.1021/acs.chemrev.8b00252.

[19]   F. Wang, S. Xiao, Y. Hou, C. Hu, L. Liu, and Y. Wu, "Electrode materials for aqueous asymmetric supercapacitors," *RSC Adv*, vol. 3, no. 32, p. 13059, 2013, doi: 10.1039/c3ra23466e.

[20]   D. P. Chatterjee and A. K. Nandi, "A review on the recent advances in hybrid supercapacitors," *J Mater Chem A Mater*, vol. 9, no. 29, pp. 15880–15918, 2021, doi: 10.1039/D1TA02505H.

[21]   E. Frackowiak, "Carbon materials for supercapacitor application," *Physical Chemistry Chemical Physics*, vol. 9, no. 15, p. 1774, 2007, doi: 10.1039/b618139m.

[22]   C. An, Y. Zhang, H. Guo, and Y. Wang, "Metal oxide-based supercapacitors: progress and prospectives," *Nanoscale Adv*, vol. 1, no. 12, pp. 4644–4658, 2019, doi: 10.1039/C9NA00543A.

[23]   N. S. George, L. Maria Jose, and A. Aravind, "Review on Transition Metal Oxides and Their Composites for Energy Storage Application," in *Updates on Supercapacitors*, IntechOpen, 2023. doi: 10.5772/intechopen.108781.

[24]   G. A. Snook, P. Kao, and A. S. Best, "Conducting-polymer-based supercapacitor devices and electrodes," *J Power Sources*, vol. 196, no. 1, pp. 1–12, Jan. 2011, doi: 10.1016/j.jpowsour.2010.06.084.

[25]   Q. Meng, K. Cai, Y. Chen, and L. Chen, "Research progress on conducting polymer based supercapacitor electrode materials," *Nano Energy*, vol. 36, pp. 268–285, Jun. 2017, doi: 10.1016/j.nanoen.2017.04.040.

[26]   W. W. Focke and G. E. Wnek, "Conduction mechanisms in polyaniline (emeraldine salt)," *J Electroanal Chem Interfacial Electrochem*, vol. 256, no. 2, pp. 343–352, Dec. 1988, doi: 10.1016/0022-0728(88)87008-6.

[27]   I. Sapurina and J. Stejskal, "The mechanism of the oxidative polymerization of aniline and the formation of supramolecular polyaniline structures," *Polym Int*, vol. 57, no. 12, pp. 1295–1325, Dec. 2008, doi: 10.1002/pi.2476.

[28] B. D. Malhotra and Md. A. Ali, "Biopolymeric Nanostructures," in *Nanomaterials for Biosensors*, Elsevier, 2018, pp. 127–144. doi: 10.1016/B978-0-323-44923-6.00004-2.

[29] G. Konwar, S. Ch. Sarma, D. Mahanta, and S. C. Peter, "Polyaniline Hybrid Nanofibers via Green Interfacial Polymerization for All-Solid-State Symmetric Supercapacitors," *ACS Omega*, vol. 5, no. 24, pp. 14494–14501, Jun. 2020, doi: 10.1021/acsomega.0c01158.

[30] D. Li, J. Huang, and R. B. Kaner, "Polyaniline Nanofibers: A Unique Polymer Nanostructure for Versatile Applications," *Acc Chem Res*, vol. 42, no. 1, pp. 135–145, Jan. 2009, doi: 10.1021/ar800080n.

[31] Y. Tan and K. Ghandi, "Kinetics and mechanism of pyrrole chemical polymerization," *Synth Met*, vol. 175, pp. 183–191, Jul. 2013, doi: 10.1016/j.synthmet.2013.05.014.

[32] N. Cheng, L. Zhang, J. Joon Kim, and T. L. Andrew, "Vapor phase organic chemistry to deposit conjugated polymer films on arbitrary substrates," *J Mater Chem C Mater*, vol. 5, no. 23, pp. 5787–5796, 2017, doi: 10.1039/C7TC00293A.

[33] C. Zhao, X. Jia, K. Shu, C. Yu, G. G. Wallace, and C. Wang, "Conducting polymer composites for unconventional solid-state supercapacitors," *J Mater Chem A Mater*, vol. 8, no. 9, pp. 4677–4699, 2020, doi: 10.1039/C9TA13432H.

[34] A. Laheäär, P. Przygocki, Q. Abbas, and F. Béguin, "Appropriate methods for evaluating the efficiency and capacitive behavior of different types of supercapacitors," *Electrochem commun*, vol. 60, pp. 21–25, Nov. 2015, doi: 10.1016/j.elecom.2015.07.022.

[35] M. Abutalip *et al.*, "Strategic Synthesis of 2D and 3D Conducting Polymers and Derived Nanocomposites," *Advanced Materials*, vol. 35, no. 5, p. 2208864, Feb. 2023, doi: 10.1002/adma.202208864.

[36] I. Y. Choi, J. Lee, H. Ahn, J. Lee, H. C. Choi, and M. J. Park, "High-Conductivity Two-Dimensional Polyaniline Nanosheets Developed on Ice Surfaces," *Angewandte Chemie International Edition*, vol. 54, no. 36, pp. 10497–10501, Sep. 2015, doi: 10.1002/anie.201503332.

[37] F. Song, J. Xu, and W. G. Hou, "Surfactant-free oil/water and bicontinuous microemulsion composed of benzene, ethanol and water," *Chinese Chemical Letters*, vol. 21, no. 7, pp. 880–883, Jul. 2010, doi: 10.1016/j.cclet.2010.01.029.

[38] M. Shabani-Nooshabadi and F. Karimian-Taheri, "Electrosynthesis of a polyaniline/zeolite nanocomposite coating on copper in a three-step process and the effect of current density on its corrosion protection performance," *RSC Adv*, vol. 5, no. 117, pp. 96601–96610, 2015, doi: 10.1039/C5RA14333K.

[39] M. C. Gupta and S. S. Umare, "Studies on Poly(o-methoxyaniline)," 1992. [Online]. Available: https://pubs.acs.org/sharingguidelines

[40] S. H. Khor, K. G. Neoh, and E. T. Kang, "Synthesis and characterization of some polyaniline–organic acceptor complexes," *J Appl Polym Sci*, vol. 40, no. 1112, pp. 2015–2025, Dec. 1990, doi: 10.1002/app.1990.070401116.

[41] S. G. Kim, J. W. Kim, H. J. Choi, M. S. Suh, M. J. Shin, and M. S. Jhon, "Synthesis and electrorheological characterization of emulsion-polymerized dodecylbenzenesulfonic acid doped polyaniline-based suspensions," *Colloid Polym Sci*, vol. 278, no. 9, pp. 894–898, Sep. 2000, doi: 10.1007/s003960000360.

[42] S. Bhadra, N. K. Singha, and D. Khastgir, "Electrochemical synthesis of polyaniline and its comparison with chemically synthesized polyaniline," *J Appl Polym Sci*, vol. 104, no. 3, pp. 1900–1904, May 2007, doi: 10.1002/app.25867.

[43] N. J. Pinto, P. D. Shah, P. K. Kahol, and B. J. McCormick, "Dielectric constant and ac conductivity in polyaniline derivatives," *Solid State Commun*, vol. 97, no. 12, pp. 1029–1031, Mar. 1996, doi: 10.1016/0038-1098(95)00853-5.

[44] A. G. MacDiarmid and A. J. Epstein, "The concept of secondary doping as applied to polyaniline," *Synth Met*, vol. 65, no. 2–3, pp. 103–116, Aug. 1994, doi: 10.1016/0379-6779(94)90171-6.

[45] D. Li, J. Liang, S. Song, and L. Li, "Highly Cross-Linked 3D ε-Fe$_2$O$_3$ Networks Organized by Ultrathin Nanosheets as High-Performance Anode Materials for Lithium-Ion Storage," *ACS Appl Nano Mater*, vol. 6, no. 4, pp. 2356–2365, Feb. 2023, doi: 10.1021/acsanm.2c04359.

[46] F. G. Souza, L. Sirelli, R. C. Michel, B. G. Soares, and M. H. Herbst, "In situ polymerization of aniline in the presence of carbon black," *J Appl Polym Sci*, vol. 102, no. 1, pp. 535–541, Oct. 2006, doi: 10.1002/app.24280.

[47] P. Vadhva *et al.*, "Electrochemical Impedance Spectroscopy for All-Solid-State Batteries: Theory, Methods and Future Outlook," *ChemElectroChem*, vol. 8, no. 11, pp. 1930–1947, Jun. 2021, doi: 10.1002/celc.202100108.

[48] H. Li *et al.*, "Carbon electrode with conductivity improvement using silver nanowires for high-performance supercapacitor," *Applied Physics A*, vol. 124, no. 11, p. 763, Nov. 2018, doi: 10.1007/s00339-018-2182-4.

[49] E. Taer *et al.*, "The relationship of surface area to cell capacitance for monolith carbon electrode from biomass materials for supercapacitor aplication," in *Journal of Physics: Conference Series*, Institute of Physics Publishing, Dec. 2018. doi: 10.1088/1742-6596/1116/3/032040.

[50] A. A. Yaqoob, M. N. M. Ibrahim, A. Ahmad, A. Khatoon, and S. H. M. Setapar, "Polyaniline-Based Materials for Supercapacitors," in *Handbook of Supercapacitor Materials*, Wiley, 2021, pp. 113–130. doi: 10.1002/9783527824779.ch4.